SEDIMENTOLOGY the journal of the International Association of Sedimentologists

Sedimentology (2022) doi: 10.1111/sed.13068

Quaternary lacustrine carbonate deposits of the Great Basin, USA: Impact of climate, tectonics and substrate

PIERRE BOUSSAGOL*, EMMANUELLE VENNIN*, ANTHONY BOUTON*,†, ADELINE ROCHE*, CHRISTOPHE THOMAZO*, CHRISTOPHE KOLODKA‡, JEAN-FRANÇOIS BUONCRISTIANI*, FABRICE MONNA§, OLIVIER MUSSET¶ and PIETER T. VISSCHER*,**

**Biogéosciences, UMR 6282 CNRS, Université Bourgogne Franche-Comté, 6 Boulevard Gabriel, 21000, Dijon, France (E-mail: pierre.boussagol@u-bourgogne.fr) (E-mail: emmanuelle.vennin@u-bourgogne.fr)*

†Socna Sols, 38 av. de la République, 21200 Beaune, France

‡MODIS Pau, 4 rue Jules Ferry, 64000, Pau, France

§UMR 6298, ArTeHiS, Université Bourgogne Franche-Comté–CNRS, 21000, Dijon, France

¶Laboratoire Interdisciplinaire Carnot de Bourgogne, UMR 6303 CNRS, Université Bourgogne Franche-Comté, 9 Avenue Alain Savary, 21000, Dijon, France

***Departments of Marine Sciences & Geosciences, University of Connecticut, Storrs, CT 06269, USA*

Associate Editor – Ying Zhou

ABSTRACT

The Great Basin included several lacustrine systems that accommodated extensive carbonate buildups: the Lahontan on the western side (dating back to 48 kyr cal BP), and the Bonneville (from 30 to 11.5 kyr cal BP) and Great Salt Lake (starting 11.5 kyr cal BP) on the eastern side of the basin. The eastern lakes show a transition from freshwater to hypersaline conditions. In contrast, the western lakes do not show any significant change from the originally prevailing freshwater conditions. Mapping of the carbonate buildups in the different lakes settings enables a comparison of a biotic versus an abiotic composition of the carbonate buildups, their morphologies and their specific spatial distributions. The morphology, size and distribution of the carbonate deposits are predominantly governed by seasonal to long-term water level fluctuations, particular geomorphological heritage, fault-induced processes, groundwater seepage and substrates. All of the lakes show a palaeoshoreline distribution with some buildups containing crusts, hemispheroid domes, and parts of complex domes resulting from climate-induced lake level variations. However, the presence of columns and complex domes made up of mixed biotic/abiotic carbonates in the western Great Basin is related to the influx of groundwater. Winnemucca Lake and Pyramid Lake contain bigger buildups than the ones observed in the eastern Great Basin lakes. The presence of these large size buildups and thinolites in the Lahontan lacustrine system are a consequence of local hydrological processes associated with influenced groundwater flows through specific sedimentary structures (for example, from springs and delta fronts) and faults. This contrast in the distribution, composition and size of the buildups between the two sides of the Great Basin suggests local changes in water chemistry (for example, $[Ca^{2+}]$) and groundwater influxes. This work provides a novel conceptual model for the formation of abiotic and/or biotic carbonate buildups in lacustrine settings.

Keywords Buildups, Great Basin, Great Salt Lake/Lake Bonneville endorheic lakes, Lahontan, microbialites, thinolites

INTRODUCTION

Porous freshwater carbonate deposits composed of microbial-dominated boundstones, bioclastic packstones and cements (for example, large-crystals) are frequently found in the Great Basin where they shape lacustrine deposits in both the Bonneville and Lahontan hydrological basins, and are referred to as tufa in the literature (Benson, 1994; Benson *et al.*, 1995; Vennin *et al.*, 2019; DeMott *et al.*, 2019b; DeMott & Scholz, 2020). A clear biotic origin for the carbonate mineralization is more easily observed in modern tufa systems than in fossil ones (Hofmann & Farmer, 2000; Schopf *et al.*, 2007) and our previous studies in the eastern Great Basin have shown that the carbonate buildups are microbially mediated (Vennin *et al.*, 2019). This abundant role for microbial activity is less evident in western Lahontan buildups due to the presence of abiotic calcite cements (for example, thinolites). The buildups in the western area have been interpreted as a continuum between the two extremes of physical (cements) and microbial (clots, micrite) precipitation (Pedley & Rogerson, 2010; Della Porta, 2015). The combination of microbially-induced precipitation (Bouton *et al.*, 2016a,b; Vanden Berg, 2019; Vennin *et al.*, 2019) and chemically-induced cements (thinolites; Shearman *et al.*, 1989; Bischoff *et al.*, 1993a; Ludwig *et al.*, 2006; Bates *et al.*, 2010; Zhou *et al.*, 2015; Purgstaller *et al.*, 2017) is referred in this study as 'hybrid carbonates' (Riding & Virgone, 2020).

Chemically-induced abiotic precipitation of carbonates depends on the physico-chemical properties of the water, that result in a specific saturation state of carbonates (Zeebe, 2012) related to CO_2 outgassing (for example, wave action), continental runoff, and relative contribution of groundwater and hydrothermal spring-derived water (Kelts & Talbot, 1990; Arenas-Abad *et al.*, 2010; Della Porta, 2015). In contrast, microbialites are formed through the mineralization of benthic microbial mats and/or the trapping and binding of sedimentary particles (Burne & Moore, 1987; Visscher *et al.*, 2022). Microbialites are produced by a complex interplay between the microbial community and its metabolic activities, the specific mechanisms of $CaCO_3$ precipitation and the surrounding (local to global) environmental conditions (Riding, 2000; Dupraz *et al.*, 2009; Arenas-Abad *et al.*, 2010; Arenas *et al.*, 2014; Bouton *et al.*, 2016a,b; Pace *et al.*, 2016; Vennin *et al.*, 2019). In sum, the contribution of abiotic versus biotic processes to carbonate precipitation depends on intrinsic (i.e. composition of the microbial communities), extrinsic (i.e. degassing, evaporation) and external controls (for example, geodynamic context, accommodation space, water quality, hydrodynamic regime, light conditions and nutrient availability; Jahnert & Collins, 2013; Bouton *et al.*, 2016b).

In the Great Basin, two different carbonate buildups have been described as shoreline-tufa and spring-associated tufa (Benson *et al.*, 1995; Bouton *et al.*, 2016a,b; Vennin *et al.*, 2019; DeMott *et al.*, 2019b). The carbonate buildup distribution is non-random (Bouton *et al.*, 2016b; Roche *et al.*, 2018; Baskin *et al.*, 2021; Vennin *et al.*, 2021) and reflects specific climatic, geodynamic and physiographic parameters. Climate-driven water level fluctuations may explain palaeoshoreline migrations as well as the distribution of some buildups in both sides of the Great Basin [Lahontan lacustrine system: Benson, 1994; Adams & Rhodes, 2019; Lake Bonneville and Great Salt Lake (GSL): Bouton *et al.*, 2016a,b; Vanden Berg, 2019; Vennin *et al.*, 2019]. Tectonics is also an additional major driver for the eastern Great Basin buildup distribution (for example, in GSL) due to the presence of normal faults (Baskin *et al.*, 2011, 2021; Bouton *et al.*, 2016a, b). Fault-controlled topographic highs and fault-related topographic falls in GSL determine the distribution of the microbial buildups (Bouton *et al.*, 2016a; Baskin *et al.*, 2021). Although, at Pyramid Lake, some of the largest buildups may be associated with faults as proposed by Eisses *et al.* (2015), most of the carbonate structures in both Winnemucca and Pyramid are not directly associated with faults. Instead, the buildups are arranged along the flexural margin of the half-graben and affected by stratigraphically-controlled groundwater flow paths (DeMott & Scholz, 2020). In addition, the substrate lithology can drive the development of the carbonate buildups because firm and stable substrates have been shown to play a physical and chemical role (i.e. through ion availability) in the microbialite development in French rivers (Roche *et al.*, 2019) and in GSL (Bouton *et al.*, 2016a; Vennin *et al.*, 2021). The role of the substrate on the development of the buildups has not been addressed in the western Great Basin.

The high degree of structural heterogeneity (physiography, substrate, faults) and the difference in size, morphology and composition of

the carbonate buildups on both sides of the Great Basin (Lahontan and Bonneville basins) will provide new insight on the multiple factors favouring their biotic and/or abiotic development. To date, no study has explained the difference in carbonate production between these lakes that otherwise share a similar climate and geodynamic evolution. The current work aims to: (i) characterize and map the distribution of different carbonate buildup morphologies; (ii) link seismic structural patterns with the development of the carbonate buildups; (iii) use the morphology and distribution of the carbonate buildups, to discuss the controlling factors involved in their development and preservation; and (iv) compare the carbonate deposition and processes in different areas at the Great Basin scale, and in particular focusing on the budget of Ca^{2+} leading to the carbonate precipitation.

GEOLOGICAL AND GEOGRAPHICAL CONTEXT

The lacustrine systems in this study are part of the Basin & Range geodynamic province (Fig. 1A). The Basin & Range includes the large hydrographic province of the Great Basin composed of several endorheic basins that spanned 520 000 km^2 at the end of the Pleistocene, when this major lake system reached its peak size (Fig. 1A; Reheis *et al.*, 2014). Two main lacustrine systems can be differentiated at this time: the Lahontan lacustrine system in the west (Benson *et al.*, 1992; DeMott *et al.*, 2019b; Roche, 2020) and the Lake Bonneville in the east (Fig. 1B and C; Vanden Berg, 2019; Vennin *et al.*, 2019; Bouton *et al.*, 2020), with areas of 52 300 km^2 and 22 300 km^2, respectively. The water level of these lakes has been subject to significant climatic-driven variations during the Pleistocene and Holocene (Fig. 2; McKenzie & Eberli, 1985; Murchison, 1989; Patrickson *et al.*, 2010). Consequently, several successive lacustrine cycles are recorded (Benson *et al.*, 1992; Oviatt & Nash, 2014; DeMott *et al.*, 2019b).

During the Pleistocene, the Lahontan lacustrine system consisted of seven pluvial lakes that were connected (Benson & Mifflin, 1986; Adams & Wesnousky, 1999; Benson *et al.*, 2013a,b; Adams & Rhodes, 2019; Roche, 2020). During the high-water level period (Lake Lahontan Highstand or Sehoo Highstand; Figs 1A, 2 and 3A), the lacustrine complex had a water volume of 2020 km^3 and a maximum depth of 270 m in the Pyramid sub-basin (Benson & Mifflin, 1986; Roche, 2020). The 48 kyr cal BP long Sehoo Highstand is the longest lacustrine and sedimentological episode of the Lahontan Lake (Benson *et al.*, 2013b). The different lakes were separated by elevation sills, including Lahontan Highstand, Darwin Pass, Emerson Pass and Mud Lake Slough. These sills determined high and/or low water levels in the system and caused periods of water level stabilization (Fig. 2; Benson, 1994). The sills are correlated to sedimentary terraces that formed during the stabilization of the water level (Fig. 3A to C; Benson, 1994). Six major terraces, eponymous to elevation sills, record the successive lake level fluctuations since the last Quaternary glaciation (Oviatt *et al.*, 1992). Remarkably, buildups are more abundant in sills than in the current shoreline.

The western part of the Lahontan lacustrine system is associated with a transtensive tectonic activity involving the movements of normal faults and discontinuous strike-slip faults (Wesnousky, 2005; Hammond *et al.*, 2011). This tectonic activity generated a succession of horsts, grabens and half-grabens, that favoured the formation of endorheic lakes with a specific geometry and extension (Stewart, 1971). Hydrothermal activity associated with the fault is present at the western part of the Lahontan lacustrine system along the Walker Lane Belt (Faulds & Hinz, 2015). The lakes are supplied by water from rivers fed by ice and snow melt from the surrounding mountains and watershed (Chambers & Miller, 2011). As a result, the water level of these endorheic lakes was directly controlled by the deglaciation that started about 15 ka (McKenzie & Eberli, 1985; Adams & Wesnousky, 1999; DeMott *et al.*, 2019b). At that time, a drastic fall of the water level can be recorded (Fig. 2; Benson *et al.*, 2013b; Adams & Rhodes, 2019). This drop in lake water level was regional as it is observed in the Bonneville Basin (Oviatt, 1997; Bouton *et al.*, 2020; Vennin *et al.*, 2021) and in the Estancia Lake (New Mexico; Allen & Anderson, 2000). This decrease in water level coincided with the beginning of the warm Bølling–Allerød climatic event (Godsey *et al.*, 2011). Remnants of plants and pollen indicate a transition from a previously cold and wet climate to cold and dry conditions, accompanied by limiting water inputs and promoting evaporation (Madsen *et al.*, 2001).

The Pyramid Lake, with an average altitude of 1157 m above sea level (masl), is fed by the Truckee River, and is the third largest perennial lake of the Great Basin. It currently covers an

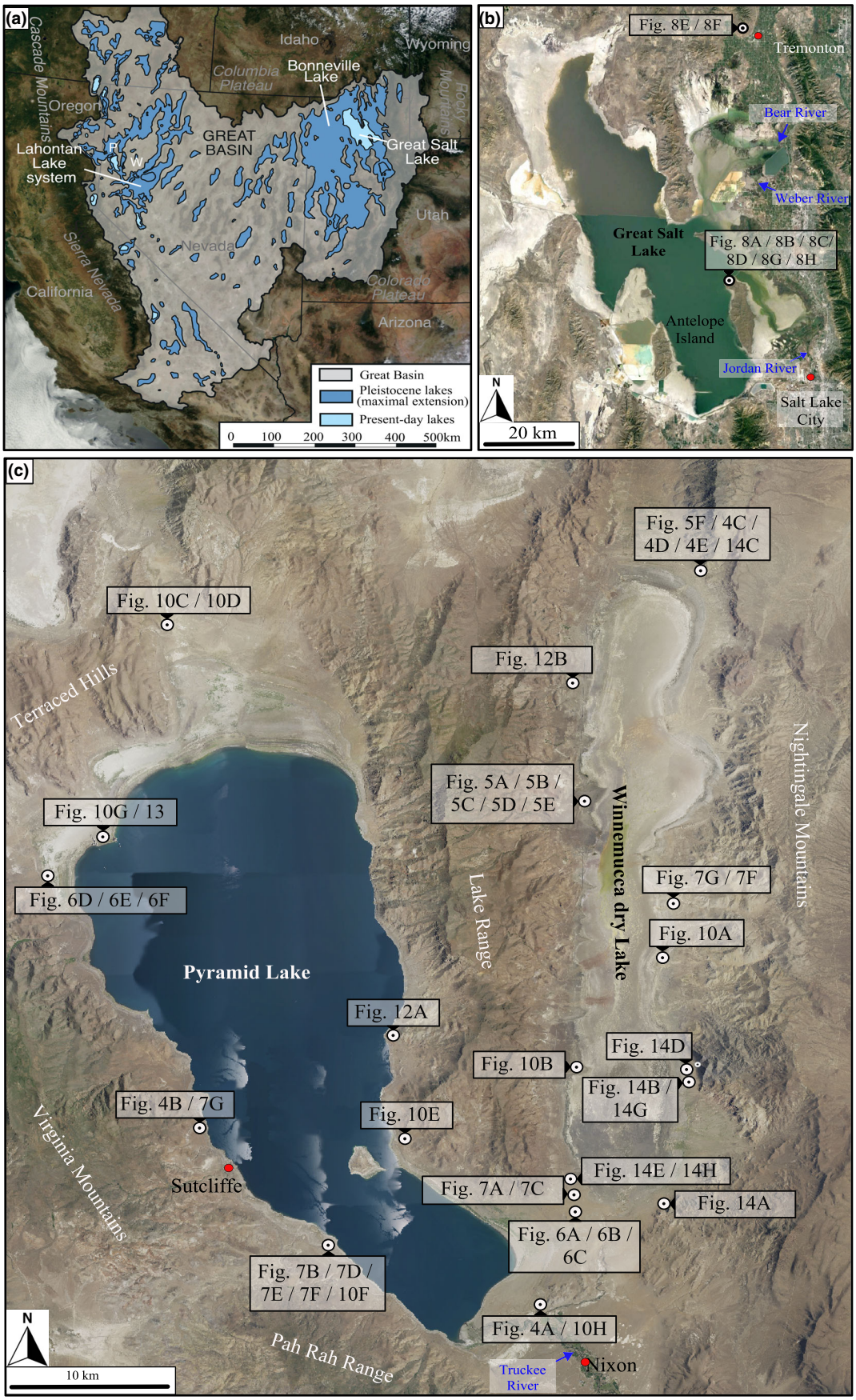

Fig. 1. (A) Satellite image [NASA Terra (Satellite EOS AM-1) 28/07/2015 – www.flashearth.com] showing the Great Basin and the maximum extents of modern and Pleistocene lakes; study areas are Lake Bonneville and Great Salt Lake located at the eastern side of the Great Basin and the Lahontan lacustrine system [Pyramid Lake (P), Winnemucca Dry Lake (W)] located at the western side (modified from Vennin *et al.*, 2019; extracted from the Morrison database, 1991). (B) Satellite image (Google Earth Pro-V7.3.4.8248, Nevada, USA. © 2021 Google) of the Great Salt Lake and Antelope Island. (C) Satellite image (NAIP 2019; www.earthexplorer.usgs.gov) with the neighbouring geological structures and showing the location of the illustrations in Figs 4, 5, 6, 7, 10, 13 and 14.

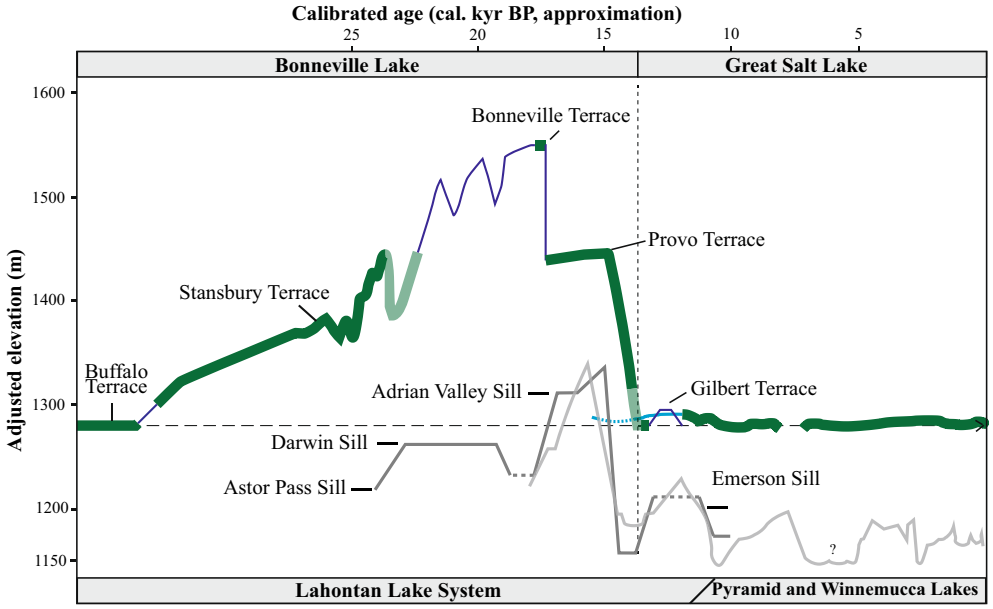

Fig. 2. Development of the lacustrine systems and their main terraces dating back 30 kyr cal BP for the eastern Great Basin: dark blue curve based on Oviatt (1997), Oviatt (2015), Patrickson *et al.* (2010) and light blue curve based on Murchison (1989); the green line of Lake Bonneville and Great Salt Lake corresponds to a synthesis of the microbial carbonate distribution. For the western Great Basin (25 kyr cal BP): dark grey curve based on Benson *et al.* (2013b) and light grey curve based on Adams & Rhodes (2019).

area of 487 km^2 with a volume of 30 km^3 and an average water depth of 62 m (Fig. 1C). Adjacent Winnemucca Dry Lake is 50 km long in the north to south direction and about 15 km wide from east to west. During the last 48 kyr cal BP, when the water level reached above the elevation of the Mud Lake Slough sill (1177–1183 masl), Pyramid Lake and Winnemucca Lake were connected in the south (Benson *et al.*, 2013b; Roche, 2020). Consequently, the two lakes have common hydrological and sedimentary histories. The climate in this area is currently arid to semi-arid with an average annual rainfall between 150 and 700 mm year^{-1} (Chambers & Miller, 2011).

Of similar age as the Lahontan lacustrine system, the Bonneville palaeolake is located at the eastern part of the Great Basin (Benson *et al.*, 1992; Vennin *et al.*, 2019). In response to climatic variations during the Pleistocene and Holocene, this palaeolake also has a complex history during the last 200 ka that comprises several lacustrine cycles (Machette *et al.*, 1992). The last cycle extended from 30 kyr cal BP to present and can be divided into two main phases; a deep Lake Bonneville phase (30 kyr to 11.5 kyr cal BP) and a shallow Great Salt Lake phase (GSL; since 11.5 kyr cal BP; Oviatt *et al.*, 1992; Vennin *et al.*, 2019; Fig. 2). Lake Bonneville is a large freshwater body with a surface area that peaked approximately 52 300 km^2 with the maximum water level at 1552 masl (Currey, 1990; Oviatt *et al.*, 1992; Godsey *et al.*, 2011). Following the period of high-water stand, the lake level of the Bonneville system repeatedly declined during different episodes

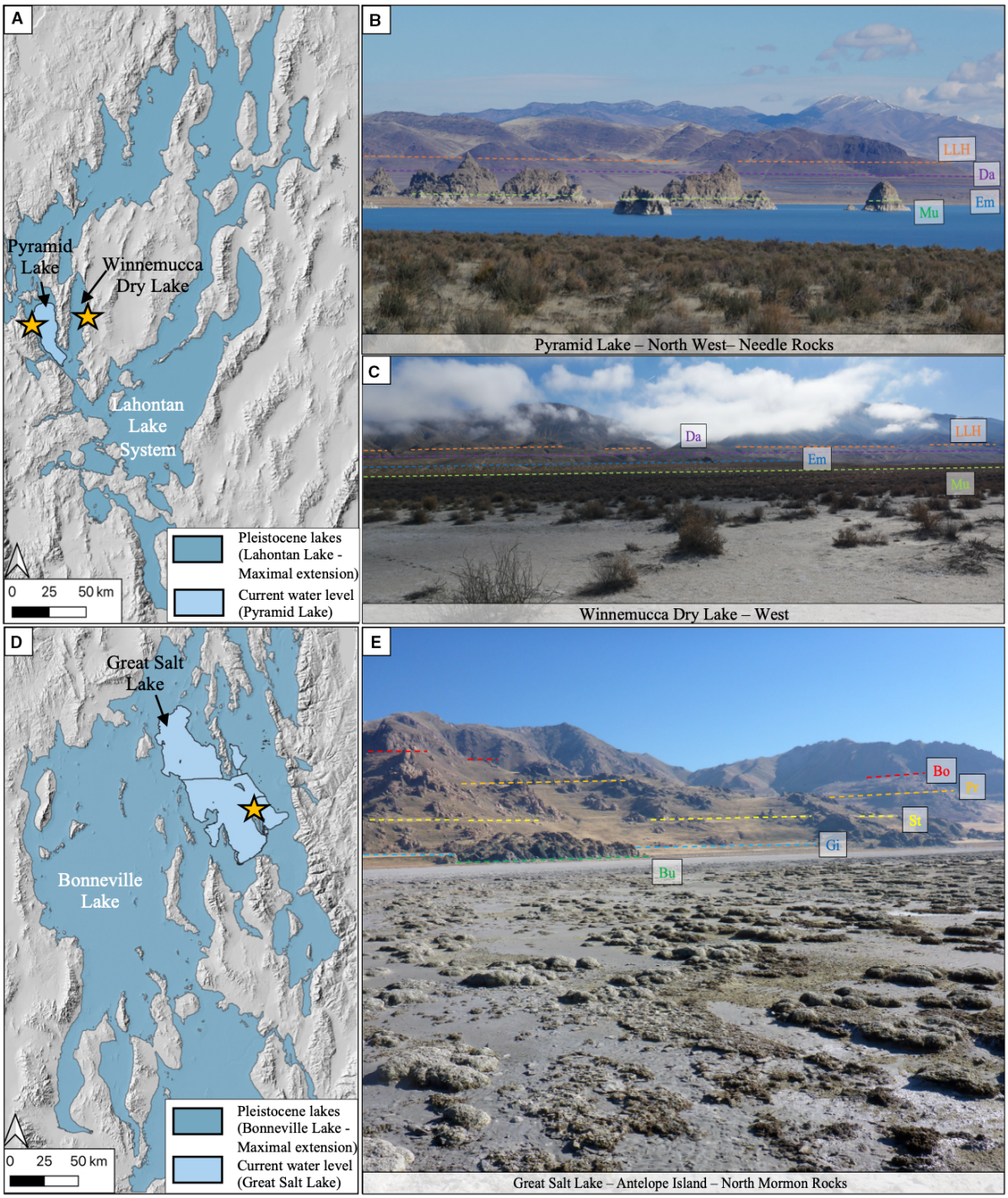

Fig. 3. (A) Digital elevation model (DEM) showing the Lahontan lacustrine system (Pyramid Lake and Winnemucca Dry Lake) and the location of various panoramas (yellow stars). Panorama of the terraces cropping out on the north-western shore of Pyramid Lake (B) and panorama of the terraces on western shore of Winnemucca Dry Lake (C); the extension of the different terraces associated with elevation sills located according to Benson *et al.* (2013a,b) and Adams & Rhodes (2019). Green line: Mud Lake sill (Mu), blue line: Emerson sill (Em), purple line: Darwin sill (Da), and orange line: Lake Lahontan high stand (LLH). (D) Digital Elevation Model (USGS 90 m state-wide, available from https://gis.utah.gov/) showing the extent of Lake Bonneville (dark blue) and Great Salt Lake (light blue). Also shows the location of the panorama (yellow star): north-western Antelope Island – north Mormon Rocks. (E) Panorama of north Mormon Rocks showing the preserved terraces from the lower to the higher elevation (Bu: Buffalo, Gi: Gilbert, St: Stansbury, Pr: Provo and Bo: Bonneville).

until only a residual lake referred to as the Great Salt Lake (GSL) remained (Vennin *et al.*, 2019). This endorheic lake measures 4480 km^2, is shallow (maximum depth around 10 m; Baskin & Allen, 2005; Baskin & Turner, 2006), hypersaline (average salinity around 130 g l^{-1}; Gwynn, 1996), currently with a mean water level reaching 1280 m above sea level (Bouton *et al.*, 2016a). During the Bonneville and GSL phases, the various episodes of water level stabilization are preserved as sedimentary terraces including the Buffalo (approximately 1292 masl), Stansbury (1350 to 1360 masl), Bonneville (1552 masl), Provo (1444 masl) and Gilberts (approximately 1295 to 1305 masl) stillstands (Fig. 3D and E). Today, the GSL undergoes water level variations mainly due to the balance between inputs from the Bear River, the Jordan River and the Weber River (Fig. 1B) and losses caused by evaporation, which contribute to increase the alkalinity and salinity values of the lake water (Bouton *et al.*, 2020).

MATERIAL AND METHODS

The carbonate deposits and their associated sediments in Pyramid Lake and Winnemucca Dry Lake, Lake Bonneville and GSL were mapped during field campaigns between 2013 and 2021. The focus was on nearshore deposits, especially those of microbial origin. The microbial deposits are described following the three scales defined by Shapiro (2000). The macrofabric (or growth morphology) characterizes the external shape of a buildup. The mesofabric defines the internal organization of the buildup as seen with the naked eye. Finally, the microfabric represents the smallest scale that can only be observed with an optical microscope (Dupraz *et al.*, 2011). In total, 750 sediment samples of microbial deposits and other carbonate sediments were collected. The mineral composition was determined by X-Ray diffractometry (XRD) with a Siemens D5000 (Siemens AG, Munich, Germany) or a Bruker D4 Endeavour diffractometer (Bruker Corporation, Billerica, MA, USA). Thin sections were viewed using polarizing microscopes (Nikon AZ100 and Axioskop; Nikon Corporation, Tokyo, Japan; Leica DMRX, Leica, Wetzlar, Germany) and with an FEI Quanta 250 (Hillsboro, Oregon, USA) environmental scanning electron microscope, using low vacuum.

Carbonate deposits of Pyramid and Winnemucca sub-basins were initially mapped at the regional scale using satellite imagery on Google Earth Pro 7.3.4 (from State of Utah, USDA Farm Service Agency and NASA; unknown remote sensors). Mapping was combined with geo-located photographs taken during the 2018 field campaign. The different sites (>1000) pinpointed on Google Earth Pro were then recorded on a GIS software package (QGIS, version 3.16.5–Hannover). The digital elevation models (DEMs) used were acquired from ASTER-GDEM V003 maps and had a spatial resolution of 30 m (www.sciencebase.gov/catalog). Aerial photomosaics (NAIP) available on the USGS website were used. The different sill elevations were obtained from the literature (Benson, 1994; Benson *et al.*, 2013b). The location of the faults was based on a compilation of literature data as well (Eisses *et al.*, 2015, USGS, Survey, Map Geology and other) and from a compilation of local geological maps (Anderson *et al.*, 2013; Drakos & Faulds, 2013). The organization and orientation of the faults was compiled from the study of seismic profiles acquired by Eisses *et al.* (2015), particularly the D01L01 profile. Similar mapping acquisition and processing was developed for the eastern Great Basin, on the north-western shore of Antilope Island (Great Salt Lake; Bouton *et al.*, 2016a,b). A statistical analysis of the relationship between the slope and carbonate structures was performed on the QGIS software (version 3.16.5–Hannover). The use of the Slope function (SAGA, Terrain Analysis) allowed us to estimate a slope value of each mapped object using 30 m DEMs. The slope data were then compiled and processed using Excel® software (version 16.58).

RESULTS

The results of this study mainly focus on the Pyramid Lake and Winnemucca Dry Lake, because GSL has already been the subject of several publications (Bouton *et al.*, 2016a,b, 2020; Pace *et al.*, 2016 Vennin *et al.*, 2019). Table 1 summarizes the data for the different carbonate buildups found along palaeoshorelines for these two lakes and are depicted in Figs 4 to 7. The main microbial-rich deposits of the eastern Lake Bonneville (Fig. 8A to D) and Great Salt Lake (Fig. 8E to H), described previously (Bouton *et al.*, 2016a,b, 2020; Vennin *et al.*, 2019), are also included in Table 1 for comparison.

Table 1. Main buildup characteristics (size, substrate, associated sedimentation, altitude range, structural context and slope) and macrofabrics, mesofabrics and microfabrics descriptions and their interpretation in terms of depositional environments for the Lahontan lacustrine system and the Lake Bonneville/Great Salt Lake.

		Macro-fabric	Description	Meso-fabric	Micro-fabric	Size	Substrate	Associated sediments	Depositional environment	Altitude range	Context	Slope	Figs
Lahontan - Pyramid (Western Basin & Range)	**Capping crusts**	***Planar***	Thin (≈ millimetre to centimetre) to thick (10–30 cm) calcitic crusts. Crusts have a smooth, draping or cascading appearance with an irregular, pustular or meandering coral-like surface	Thick: Clotted to columnar Thin: Structureless to laminated	Thick: Hybrid filament and peloid Thin: Micrite and peloid	Thickness: 2 to 30 cm	Thick: basalt or granodiorite cliffs Thin: pebbles, cobbles, boulders, basalt cliffs, fossil microbialites	None	Shore and palaeoshorelines	1216 to 1330 masl	–	Moderate to steep (from 5 to 90%; average 15 to 45%)	4C, 4D, 4E
	Small-scale structures	***Lobate***	Crusts composed of multiple lobate structures, stacking on each other. Lobes are pendulous downward structures, or ascending in "bird's nest" or vasque	Clotted to laminated	Peloids (in clotted) Micrite (in laminated)	Thickness: multi-decimetre to metre Extension: metres to hundreds of metres	Basalt, conglomerates, thick planar crust. On surface of large-scale structures such as columns	None	Shore and palaeoshorelines	1174 to 1330 masl	–	Moderate to steep (from 5 to 90%; average 15 to 45%)	4A, 4B, 4C, 4D, 4F, 4G
	Isolated build-up	***Cow-pie***	Irregular discoid structures composed of successive laminated layers. The external surface can be pustular to smooth	Laminated to columnar	Hybrid column and micrite	Diameter: few decimetres Height: 20 cm	Sand	Mud, sand	Shore and palaeoshorelines	1153 to 1165 masl	–	Gentle (0 to 3%)	–
		Tubular bush	Accumulation of small tubes (spaghetti-like) in bush. Tubes are 1–2 mm in diameter with an empty centre (300–400 μm in diameter) with calcitic walls. They are associated with gastropods and disarticulated ostracode shells	Tubular	Filaments	Diameter: 1 to 2 mm	–	Mud, sand	Shore and palaeoshorelines	1205 masl	–	Gentle (0 to 3%)	–

Table 1. (continued)

	Macro-fabric	Description	Meso-fabric	Micro-fabric	Size	Substrate	Associated sediments	Depositional environment	Altitude range	Context	Slope	Figs
	Thinolites and microbial	Flattened hemispheroid shapes with successive concentric layers	Inner layers: stick crystals Intermediate layers: clotted to columnar Outermost layers: laminated	Thinolite pseudomorphs (scalenohedra calcite crystals), peloids, filaments, micrite, hybrid fan-like	Diameter: 0.5 to 5.0 m; Height: up to 0.5 m	Thinolites (?) for the microbialites and sand to silt and micro-conglomerate for whole hemi-spheroid	Mud, sand, Cow-pie and Tubular bush	Shore and palaeoshorelines. Evaporation conditions?	1158 to 1180 masl	Faults (?)	Gentle (0.8 to 3.5%)	5A to 5E, 10A, 10B
Large-scale structures	***Microbial***	Dome shape with a wall composed of multiple lobate calcite structures, stacking on one another	Clotted to laminated	Peloids (in clotted) Micrite (in laminated)	Diameter: 3 to 6 m Height: up to 0.5 m	Basalt, Ryolites. Thick planar crust, and complex domes	Mud, sand	Shore and palaeoshorelines	1221 to 1300 masl	–	Gentle to moderate (from 0 to 32; average 10 to 20%)	5F, 7A, 10C to 10E
Hemispheroid domes	**Columns**	Erected columns, isolated or fused, with central pipes. Pipes pass laterally to lobate and apical pillow-shape structures. Some structures are covered by thick lobate structures inclined at 45°, stacked vertically on top of one another	Pipes in centre: clotted in the central part and laminated to columnar outward Lobate and domal associated structures: clotted, evolving into branching, then columnar and laminated layers	Peloids and filamentous (outward of pipe) Peloids branching, laminated peloids and micrite (Lobate and domal structures)	Diameter: 5 to 150 m Height: 10 to 90 m	Sands	Mud, sand and micro-conglomerates	Shore, palaeoshorelines and distal shore	1158 to 1266 masl	Faults and hydrothermal springs (?)	Gentle (0 to 11%)	6, 10G
	Complex domes	Isolated or merging domes, spheroid to mushroom-shaped structures composed of decimetre- cylinder or barrel topped by a metric dome. Domes are frequently	Pipe in centre: Clotted core, encrusted by a laminated layer evolving into columnar fabrics Concentric layers: stick	Disorganized scalenohedra calcite, or filaments and peloids (Clotted). Thinolite crystals and micrite (Hybrid)	Diameter up to 3 m	Conglomerates	Mud, sand	Shore and palaeoshorelines	1170 to 1190 and 1205 masl	Faults and hydrothermal springs (?) and substrate diffusion (?)	Gentle (0 to 14%)	7, 10F, 13

Table 1. (continued)

		Macro-fabric	Description	Meso-fabric	Micro-fabric	Size	Substrate	Associated sediments	Depositional environment	Altitude range	Context	Slope	Figs
			stacked. Composed of concentrically layers around a central pipe	crystal (thinolites), Hybrid layer (stick crystal and columnar). The outer layer capped by a columnar mesofabric	Organized peloids, micrite and hybrid column and peloid								
Bonneville phase 30 000 to 11 500 ^{14}C BP	**Small-scale structures**	**Capping crusts**	***Columnar crusts***	Isolated to fused columns organized in continuous and flat capping crusts	Clotted and laminated	Peloids, micritic laminae, microbial filaments	Thickness: 3 to 10 cm, Extension: 10 to 100 m	Previous microbial crusts or directly on Precambrian and Palaeozoic substrates, Conglomerates, botryoidal cements	Mud, sand	Slopes and onshore upon (terrace)	1280 to 1552 masl (Bonneville terraces)	–	Gentle to steep (0 to 90%)	8A
			Bushy-cauliflower	Layers composed of bushes and showing either a flat surface or an external cauliflower structure	Clotted	Peloids, micritic laminae, microbial filaments	Width: 2 to 10 cm Thickness: 5 to 20 cm	Previous microbial crusts or directly on Precambrian and Palaeozoic substrates, Conglomerates, botryoidal cements	Mud, sand	Slopes and onshore upon (terrace)	1280 to 1552 masl (Bonneville terraces)	–	Gentle to steep (0 to 90%)	8A, 8B
			Laminar	Flat, undulated to domal	Laminated	Micritic laminae	Thickness: 0.5 to 5.0 cm	Palaeozoic substrates, conglomerates	Mud, sand	Slopes and onshore upon (terrace)	1280 to 1552 masl (Bonneville terraces)	–	Gentle to steep (0% to 90%)	–
	Small scale structures	**Microbial cements**		Cluster of peloids rimmed by fibrous cements	Clotted	Peloids	Thickness: up to 2 cm	Conglomerates, botryoidal cements	Mud, sand	Slopes and onshore upon (terrace)	1280 to 1552 masl (Bonneville terraces)	–	Gentle to steep (0 to 90%)	–
Great Salt Lake Since 11 500 ^{14}C BP		**Oncoids**		Popcorn structures, reworked fragments of microbial mat and microbialites	Clotted	Peloids, coccoids	Diameter: 1 mm to 2 cm	Sands (ooids, quartz)	Mud, sand	Onshore, concentrated on the shoreline	1278 masl (Present lake level)	–	Gentle (0 to 3%)	–

Table 1. (continued)

	Macro-fabric	Description	Meso-fabric	Micro-fabric	Size	Substrate	Associated sediments	Depositional environment	Altitude range	Context	Slope	Figs
	Mimetic substrate crusts	Irregular flat cemented crust	Clotted	Peloids	Thickness: up to 2 cm	Sands (ooids, oncoids, quartz), micro-conglomerates, and all fossil microbial structures, desiccation cracks	Mud, sand	Shallow lake environment	1278 masl (Present lake level)	–	Gentle (0 to 3%)	–
	Cow-pie	Irregular to planar laminae, stacked laminae and coalescent ridge contact between the different cow-pie. Hemispheric section; hollow interior. The central part of cow-pie can be frequently truncated in the exposed area with an erosion surface locally covered by a new cow-pie growing phase	Laminated to clotted	Micritic laminae, peloids, coccoids	Thickness: up to 10 cm Width: few decimetres to metres Extension (coalescent structures): tens to hundreds of metres	Sands (ooids, oncoids), boulders, local substratum (e.g. Cambrian), covering fossil microbialites	Mud, sand	Shore and palaeoshorelines	1278 masl (Present lake level)	–	Gentle (0 to 3%)	8F
	Stromatolitic domes and columns	Circular section; single to merging structures; intense trapping and binding	Clotted and laminated	Peloids, coccoids, micritic laminae	Diameter: 10 to 50 cm Thickness: 5 cm to 2 m Extension (coalescent structures): tens to hundreds of metres	Ooid, micro-conglomerates and cow-pie structures	Mud, sand	Shore (initial growing phase) to deep lake	1278 masl (Present lake level)	–	Gentle (0 to 3%)	8E, 8F, 8G, 8H

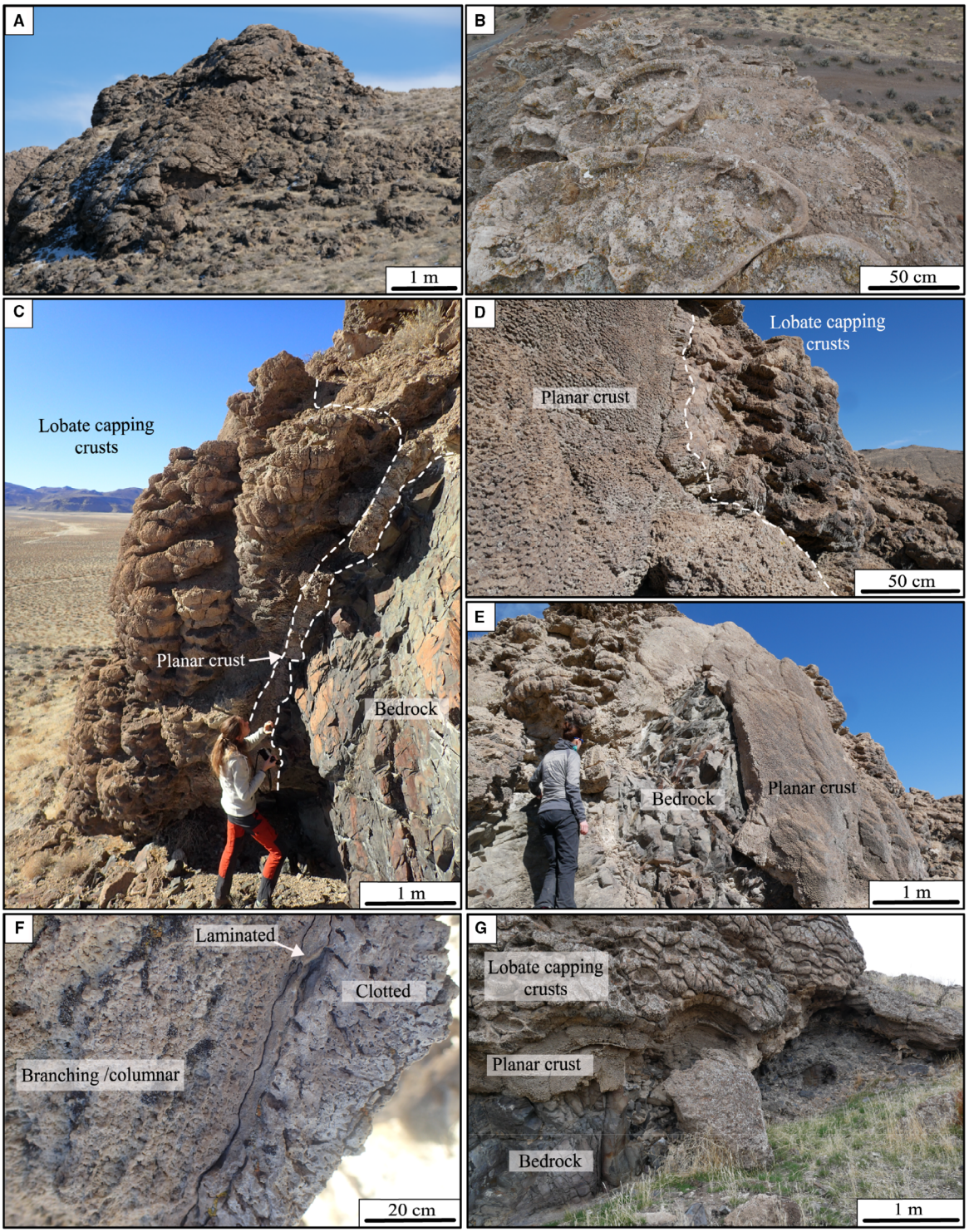

Fig. 4. Capping crusts (see location in Fig. 1C). (A) Lobate crusts that appear to flow over the substrate and completely covering a rock promontory (top to bottom vertical growth). (B) Top view of a superposition of lobate crusts characterized by a large-scale cup morphology (up to 2–3 m large) at 1205 m (Darwin Sill). (C) Encrusted promontory; the vertical bedrock is encrusted by a planar crust itself covered by lobate ("bird's-nest") crusts with a small-scale cup morphology (10–30 cm large) following a bottom to top vertical growth; the transition between the planar and the lobate crusts are illustrated on (D) and (E). (F) Transition of a planar microbial-rich crust into branching/columnar, thin-laminated to clotted mesofabrics. (G) Transition from planar to lobate crusts developed upon a basaltic substrate.

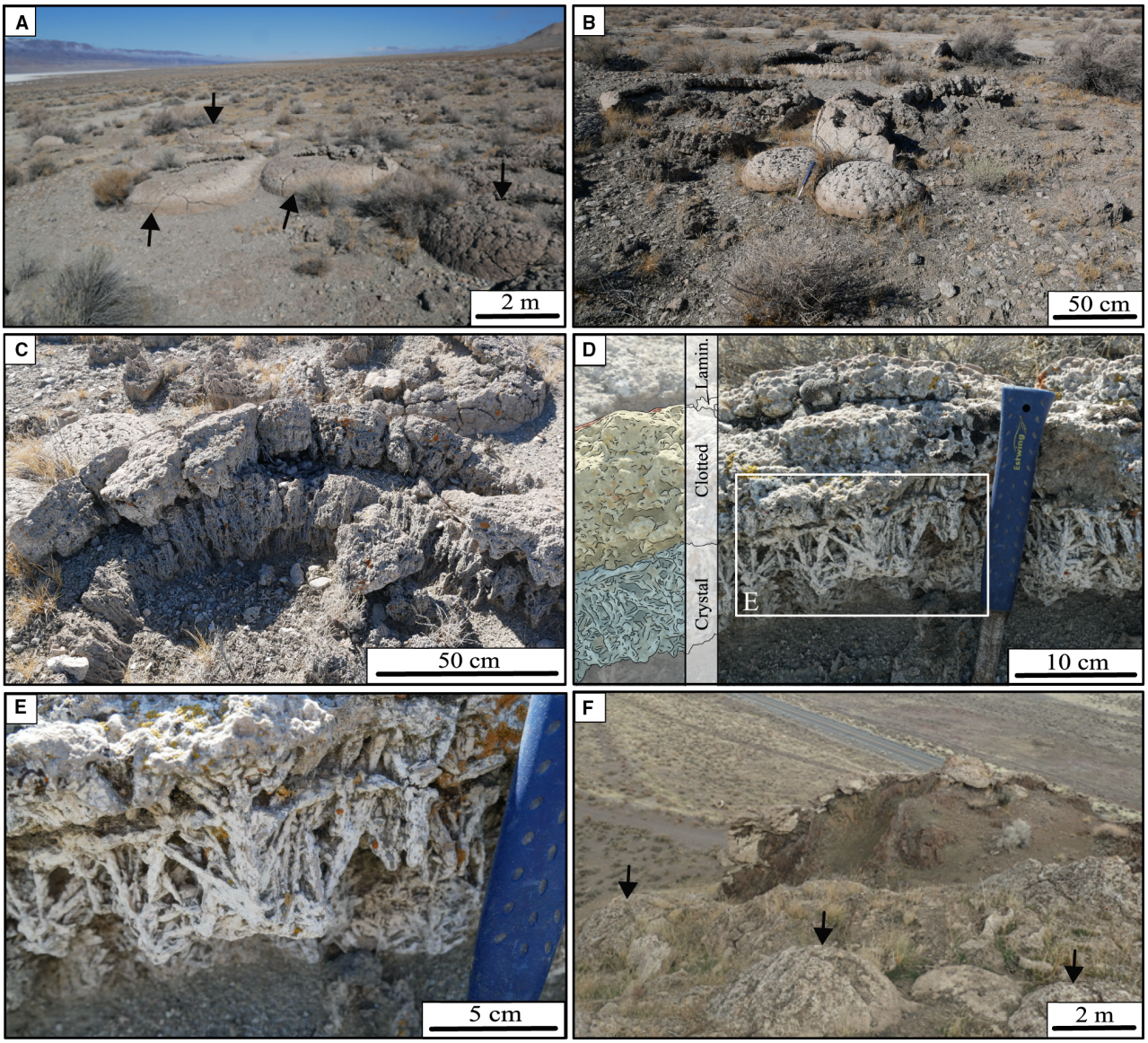

Fig. 5. Hemispheroid domes (see localization on Fig. 1C). (A) Panorama of the western shore of Winnemucca Dry Lake showing some clustered thinolite-rich hemispheroid domes. (B) Thinolite-rich hemispheroidal domes in different states of preservation. In the front, the domes are well-preserved. In contrast, in the background, they are strongly altered, showing an empty ring shape. (C) and (D) Close-up views of the thinolite-rich hemispheric domes revealing three main mesofabrics: acicular crystals (Crystal), clotted and then laminated (Lamin.). (E) Zoom of the acicular crystals (thinolite) encrusted by the microbialites. (F) Example of microbial hemispheroid domes (black arrows) developed on the palaeoshoreline of Pyramid Lake (elevation: *ca* 1200 masl).

Fabrics of the microbial deposits

Pyramid Lake and Winnemucca Dry Lake provide an important diversity of carbonate buildups with respect to size, shape and distribution. Two groups comprised of a total of five major macrofabrics could be defined: (i) small-scale structures such as capping crusts (Fig. 4), isolated buildups and hemispheroid domes (Fig. 5); and (ii) large-scale structures including columns (Fig. 6) and complex domes (Fig. 7). These macrofabrics were composed of one or several mesofabrics divided into seven sub-categories including: (i) clotted; (ii) laminated; (iii) structureless; (iv) branching; (v) columnar; (vi) acicular crystals; (vii) tubular; and (viii) hybrid composed at least of two different mesofabrics.

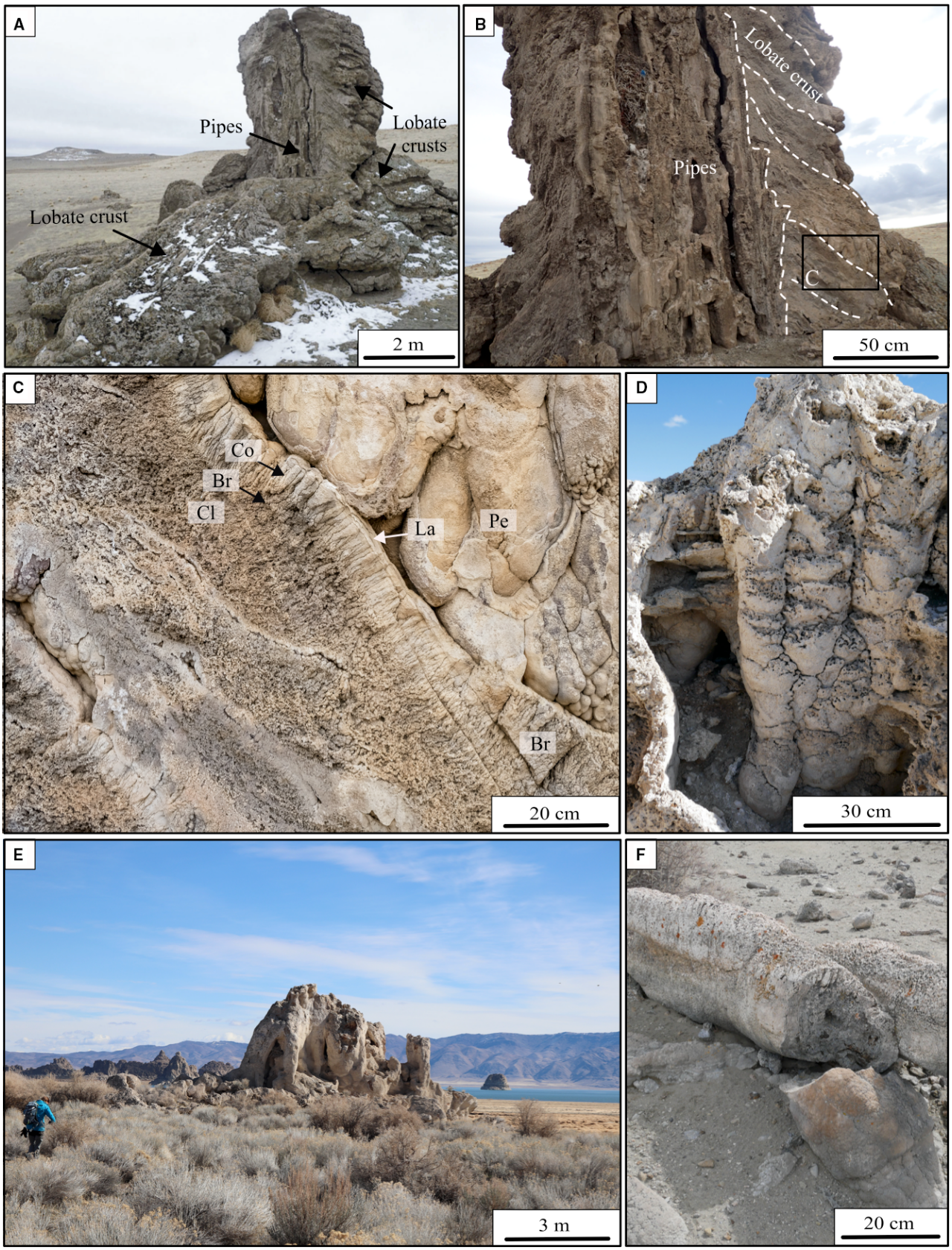

Fig. 6. Columns (see localization on Fig. 1C). (A) Columnar structure (interpreted as a chimney) on the south-western shore of Winnemucca Dry Lake. The broken face of the column reveals its internal structure and notably the pipes of the inner part [see (B) for details] and the development of microbial lobate crusts observed on the edges of the column with a succession of the following mesofabrics: peloidal (Pe), laminated (La), branching (Br), columnar (Co), clotted (Cl); see (C) for details. (D) A close-up view of the inner interior of a column showing the clustering of pipes forming the core of the large structure cropping out on the shore of Pyramid Lake (E). (F) A fallen individual pipe occurring in the vicinity of the columnar structure shown in (E).

Based on thin section analyses, five main microfabrics were identified (see Table 1 for description): (i) thinolites as scalenohedral calcite (Fig. 9A to C); (ii) hybrid of the different microfabrics (Fig. 9D and 9E); (iii) filaments (Fig. 9D); (iv) micrite (Fig. 9E and F); and (v) peloids (Fig. 9F to H).

Capping crust (Fig. 4)

Capping crusts typically cover a firm and stable substrate composed of basaltic, granitic rock and/or pre-existing carbonate structures such as domes and columns (Figs 4A to E and 6A to C). Two types could be distinguished based on their morphology and mesofabric: (i) planar crusts (Fig. 4C to G); and (ii) lobate crusts (Fig. 4A, 4B, 4C and 4G). (i) planar crusts uniformly cover the substrate. They are composed of successive millimetre to centimetre-thick layers either with a structureless or laminated mesofabric or a thick crust with a clotted to columnar mesofabric (Fig. 4F). (ii) lobate crusts are mostly observed covering the planar crusts. They show a succession of mesofabrics that from the core outward is composed of clots, transitioning into branching and then centimetre-thick layers of columnar and laminated mesofabrics (Fig. 6B and 6C). When they are not suspended, the crusts resemble the "bird's-nest" lobes of DeMott & Scholz (2020) (Fig. 4C). They are typically organized in an upward growing pattern with a progressive overlap of the underlying structure (Fig. 4A to G). These crusts are very similar to the capping crusts formed during the Bonneville phase in the eastern Great Basin, although the latter are more diverse in morphology [i.e. columnar crusts (Fig. 8A), bushy-cauliflower (Fig. 8A and B) and lobate-shaped microbial crusts (Fig. 8C and 8D)].

Isolated buildups

The isolated buildups correspond to cow pie and tubular bush morphologies. They could only be observed occasionally in Winnemucca and thus will not be discussed further here (see Table 1 for details).

Hemispheroid domes (Fig. 5)

The hemispheroid domes form flattened buildups with a positive relief on the shore. Two categories could be distinguished according to their mesofabrics and microfabrics:

1 Thinolite-rich hemispheroid domes (Fig. 5A to E) contain an empty core and a wall made of successive multiple centimetre-thick layers composed of three mesofabrics, which are from the centre outwards: a layer of acicular crystal mesofabrics (thinolites) covered by a layer of clotted mesofabrics and then a thin micritic laminated crust, which encrusts the entire buildups (Fig. 5C to E). The eroded hemispheroids are comparable to the 'ring bioherms' described by Vanden Berg (2019). Thinolites, which were considered as pseudomorphs of ikaite by calcite, were a common mineral phase in both Pyramid and Winnemucca sub-basins (Fig. 9A to C; Benson *et al.*, 2013b; DeMott *et al.*, 2019a,b). Thinolites develop directly on sand and fine-grained sediments in a radiating pattern, distal of the hemispheroid centre. The acicular thinolite crystals have a long axis ranging from millimetres to decimetres (Fig. 5A to E). They are organized in aggregated sheets which form vuggy open boxworks (Shearman *et al.*, 1989).

2 Microbial hemispheroid domes (Fig. 5F) can exceed 3 m in diameter and cover firm and stable substrates composed of basalt, granite and pre-existing carbonate buildups such as columns and complex domes. These structures have clotted to laminated mesofabrics, similar to the lobate capping crusts (Table 1). The surface of these domes is composed of multiple lobate calcite structures stacked on top of one another. These domes are very similar to the microbial-rich domes and columns formed during the GSL phase in the eastern Great Basin (Fig. 8E to H; Table 1).

Columns (Fig. 6)

Columns are several metre high erect buildups either isolated or coalescing (Fig. 6A to E). These buildups are typically 5 to 9 m in diameter and

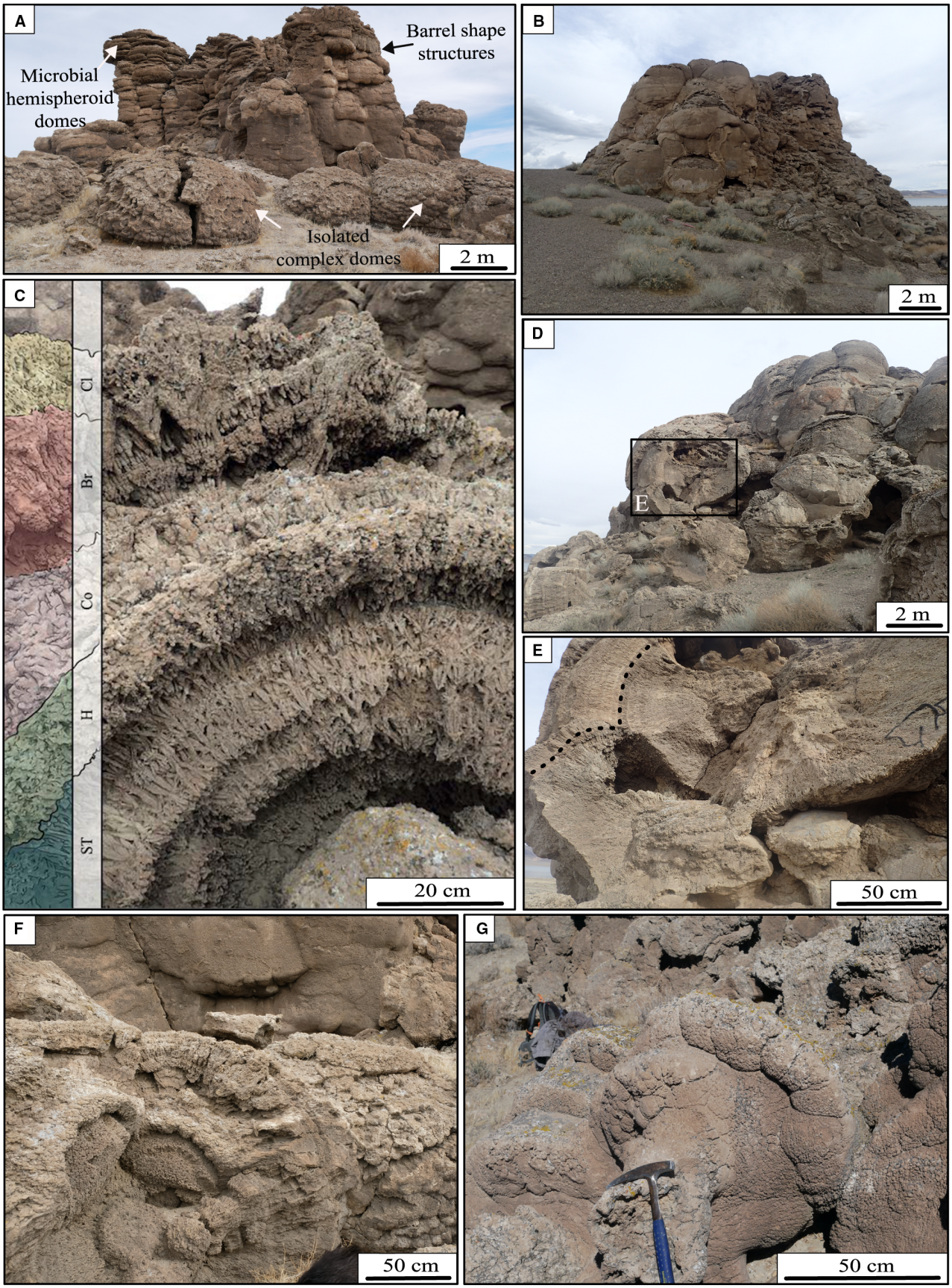

Fig. 7. Complex domes (see Fig. 1C for location). (A) Illustration of complex domes developed on the western shore of Winnemucca Dry Lake. In the front, isolated complex domes with a "bird's-nest" structure on the domal flanks. In the back, several complex domes with barrel morphologies forming columnar-like structures. (B) Illustration of Indian Head Rock occurring on the south-western shore of Pyramid Lake; coalescent complex domes are detailed in (C), (D) and (E). A close-up view (C) of a broken complex dome revealing four main concentric mesofabrics [sticked acicular crystal of thinolite (ST)], hybrid (H), columnar (Co), branching (Br), clotted (Cl) and illustrating the coalescence of some neighbouring complex domes (D) and (E). (F) A close-up view of the central part of a dome, composed of thinolite acicular crystals lacking a central pipe. (G) Complex mushroom-shaped dome associated with other rounded and barrel-shaped structures.

between 10 and 15 m high. Some buildups can reach tens of metres in height, particularly in the north-east of Pyramid Lake and are referred to as chimneys or towers, such as the Needle Rocks (Benson, 1994; DeMott *et al.*, 2019b). The outer walls of the buildups are smooth and bulbous and sometimes covered by draping crusts (Fig. 6A to C). The internal structure shows a core composed of thin pipes (a few centimetres in diameter; see Fig. 6B, 6D and 6F). From the central core outward, the column has inclined lobate structures that are superimposed and evolve, from the base to the top, into hemispheroid domes (Fig. 6A to C). The internal section of lobes is composed of a clotted mesofabric, evolving outward from branching to columnar. They are frequently encrusted by a laminated layer (Roche, 2020). Unlike some of the complex domes that form around columns and chimneys described by Brasier *et al.* (2018) in Mono Lake, these columns do not contain thinolite.

Complex domes (Fig. 7)

Complex domes are composed of accumulations of spheroidal to barrel shape buildups with dimensions of up to 3 m in diameter and height. The macrofabric resembles that of the mounds and barrels described by DeMott & Scholz (2020). The surface of these domes can be smooth to rough (Fig. 7A and B). These domes are occasionally covered with lobate, cup-shaped crusts. The stacked lobate structures resemble a turtle shell or form an inverted bowl (Fig. 7A to G). The domes are of varying size, ranging from a few metres in isolated complexes to tens of metres, especially on the shores of Pyramid Lake (i.e. Pelican Point and Indian Rock, Fig. 7B).

Complex domes are composed of concentric layers with different mesofabrics surrounding a central pipe-like structure (Fig. 7C to F). Where present, the pipes are typically single (up to 10 cm in diameter) and made up of several mesofabrics from the centre outward: a dark porous clotted core, encrusted by a laminated millimetre-thick layer. Apart from the pipes, several layers of thinolite-rich mesofabric transition outward into columnar mesofabrics (thinolites, up to 50 cm in thickness; Fig. 7C). These layers are capped by branching and finally clotted mesofabrics. In some of the complex domes the thinolites are absent and clotted and/or branching microbial mesofabrics dominate.

Mapping of carbonate buildups in both Winnemucca and Pyramid sub-basins

Approximately 1000 carbonate macrofabrics (capping crusts, hemispheroid domes, columns and complex domes) were mapped along the margins of the Pyramid Lake and Winnemucca Lake using satellite imagery, and classified based on their dominant morphology and altitude range (Figs 10 and 11). The carbonate buildups are concentrated on the western shores of the lakes at an elevation of approximately 1150 to 1330 masl. This elevation range is consistent with a common history of the Lahontan lacustrine system until the lakes were disconnected. The macrofabrics described above were mapped based on the resolution of the imagery and thus only the >1 m carbonate structures could be included. The mapping showed that lobate and planar crusts frequently co-occur (red points, Fig. 11A and 11B).

Capping crusts (red circles, Fig. 11A and 11B)

Capping crusts are the most common carbonate structures on the shores of both Pyramid Lake and Winnemucca Lake. The planar and lobate crusts are superimposed and are abundant between 1175 masl and 1330 masl. These carbonate crusts are found up to 1330 masl, which is the highest water level reached by the Lahontan lacustrine system. These crusts are ubiquitous, with a distribution ranging from flat surfaces to vertical walls at 5 to 90° slopes. In addition, they are frequently encrusting rocky promontories, or spurs and can be present at other carbonate structures as well (Figs 10C, 10D, 10E, 10H, 11A and 11B).

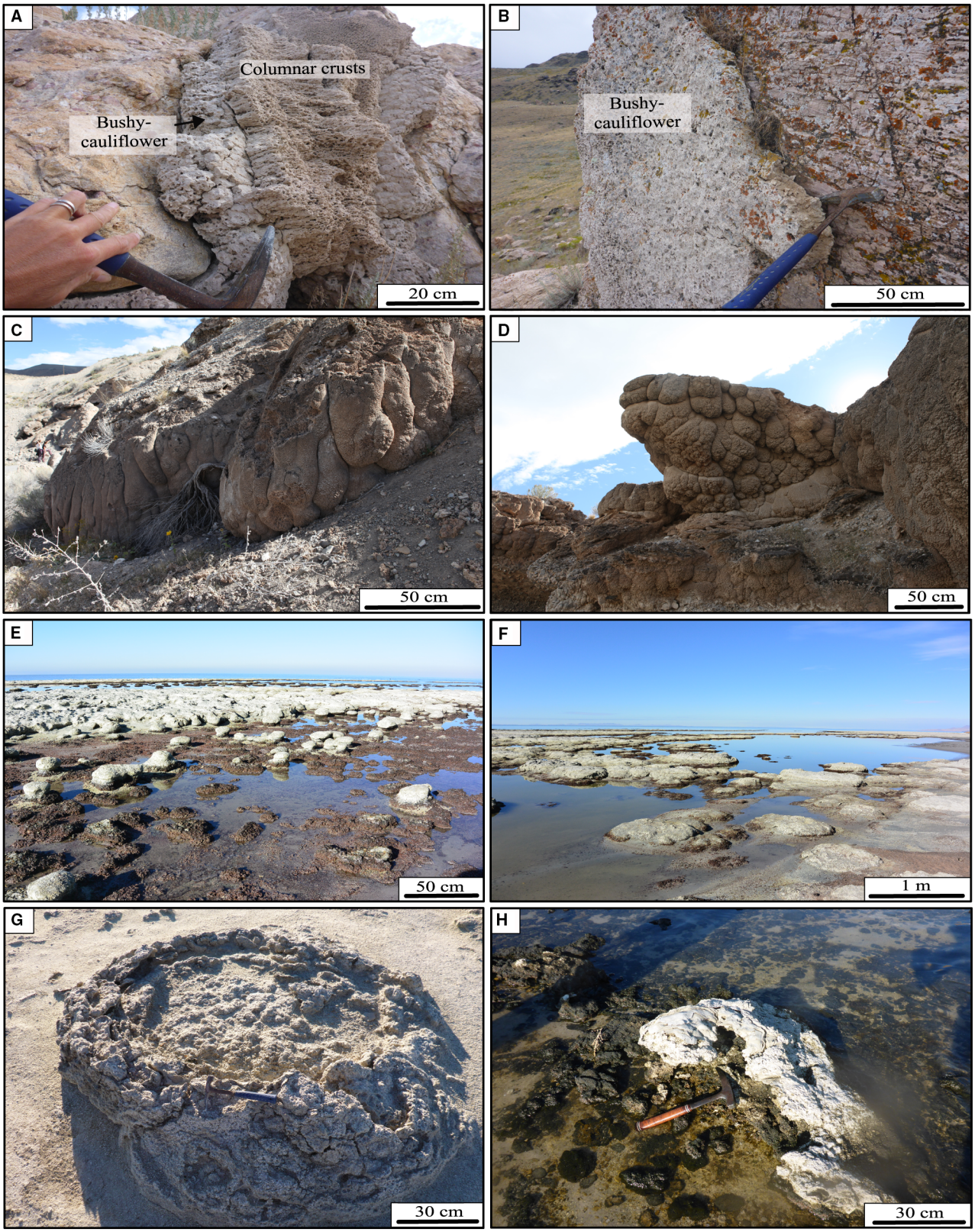

Fig. 8. Illustration of microbial deposits of Lake Bonneville and Great Salt Lake (localization on Figs 1 and 3; see Vennin *et al.*, 2019, for details and dating). (A) and (B) Examples of a capping crust at the transition of the Stansbury and the Provo terraces at Mormon Rocks (Bonneville phase) showing either a two-step growing crust (A) with a transition from a poorly structured macrofabric to a columnar microfabric (below the Stansbury terrace at Mormon Rocks) or a single step growing crust made up of a bushy-cauliflower mesofabric (B) grown on a Precambrian substrate. (C) and (D) Lobate-shaped microbial crusts encrusting a conglomerate foreset of a Gilbert delta (Tremonton area, Fig. 1B). (E) Domes and columns of the modern Great Salt Lake in a low water level configuration (Buffalo Point; November 2017; Fig. 1B). (F) Transition from dome shaped microbialites to the cow-pie structures developed near the shore. (G) Eroded domal structure observed on the shore of the Great Salt Lake, with a younger crust in the central part. (H) Detail of a microbialite showing a laminar stromatolites and clotted thrombolites, the upper part is fully mineralized whereas the greenish layer is modern microbial crust.

Thinolite-rich hemispheroid domes (yellow circles, Fig. 11A and 11B)

Thinolite-rich hemispheroid domes are isolated and aligned along the palaeoshorelines, on at least ten individual altitudes between 1158 masl and 1183 masl corresponding to Mud Lake sill elevation (Figs 5, 11A and 11B; Benson, 1994; Roche, 2020). These domes can be seen in aerial view as domes or ring shapes (Figs 5, 10A and 10B). These carbonate macrofabrics are well-developed on the shores of the Winnemucca Dry Lake, generally in low-sloped areas (0–6°) but are absent at Pyramid Lake. Thinolite-rich hemispheroids are the structures present at the lowest elevation level of Winnemucca Lake and develop on a sandy to microconglomeratic substrate referred to as beach deposits (Figs 5A, 10A and 10B). These clastic deposits resemble the beach ridges described for the Turkana Lake (Schuster & Nutz, 2018).

Microbial hemispheroid domes (green circles, Fig. 11A and 11B)

Microbial hemispheroid domes are distributed along the palaeoshorelines of both Pyramid Lake and Winnemucca Lake. These structures are particularly common on the western side of Pyramid Lake and Winnemucca Lake and on the northern and south-western borders of Pyramid Lake and are present at higher altitude than thinolite-rich hemispheroid domes, typically between 1200 masl and 1295 masl. Most of these domes are found at around 1265 masl at the elevation of the Darwin sill terrace (Figs 5F, 11A and 11B). They are abundant on flat or slightly sloped areas of the shorelines (0–30°; Fig. 10C and 10D), and on topographical highs (palaeodeltas and rhyolithic spurs; Fig. 10E) and overlap underlying carbonate structures such as complex domes and columns (Fig. 7A). When the slopes are steeper, these domes are laterally and vertically replaced by capping crusts (Fig. 10C and 10D).

Columns (white circles, Fig. 11C and 11D)

Columns comprise the tallest (up to 80 m) of the carbonate structures at Pyramid Lake, where they are abundant on the western gentle slopes (0–11°), up to 150 m width. These structures are smaller at Winnemucca Dry Lake (10 m high and 5 m in diameter), where they only occur in the south-western area of the lake. The columns are frequently flanked by complex domes with a lesser relief. Their distribution starts at 1158 masl elevation and ends at 1266 masl (Needle Rocks and Pyramid Island; Fig. 11C and D). These carbonates develop on and extend laterally into sands and muds. They are frequently isolated and are generally aligned along normal faults (Figs 10G and 12).

Complex domes (purple circles, Fig. 11C and 11D)

Complex domes form metre-scale buildups by fusing metre-wide and metre-high individual domes (Figs 7A, 7B and 10F; 'barrels' according DeMott *et al.*, 2019b). These structures form belts on flat or low-sloped areas (0–13°), along shorelines between 1170 masl and 1190 masl (dark purple circles) and at 1205 masl (light purple circles). The complex domes are distributed in patches close to apparent faults (Fig. 13A) and/or modern springs, often associated with fossil lobe-shaped structures (Fig. 13B). The largest of the complex domes are shown in Fig. 11C and 11D.

Mapping of the geological substrate in both Winnemucca and Pyramid sub-basins

Watershed substrates

The watershed is predominantly composed of igneous, metamorphic and sedimentary rocks (Figs 11B, 11D and 14A to D). The north-western area of the Winnemucca sub-basin is dominated by basalts, andesites and dacites (Fig 11B; Van Buer, 2012; Anderson *et al.*, 2013;

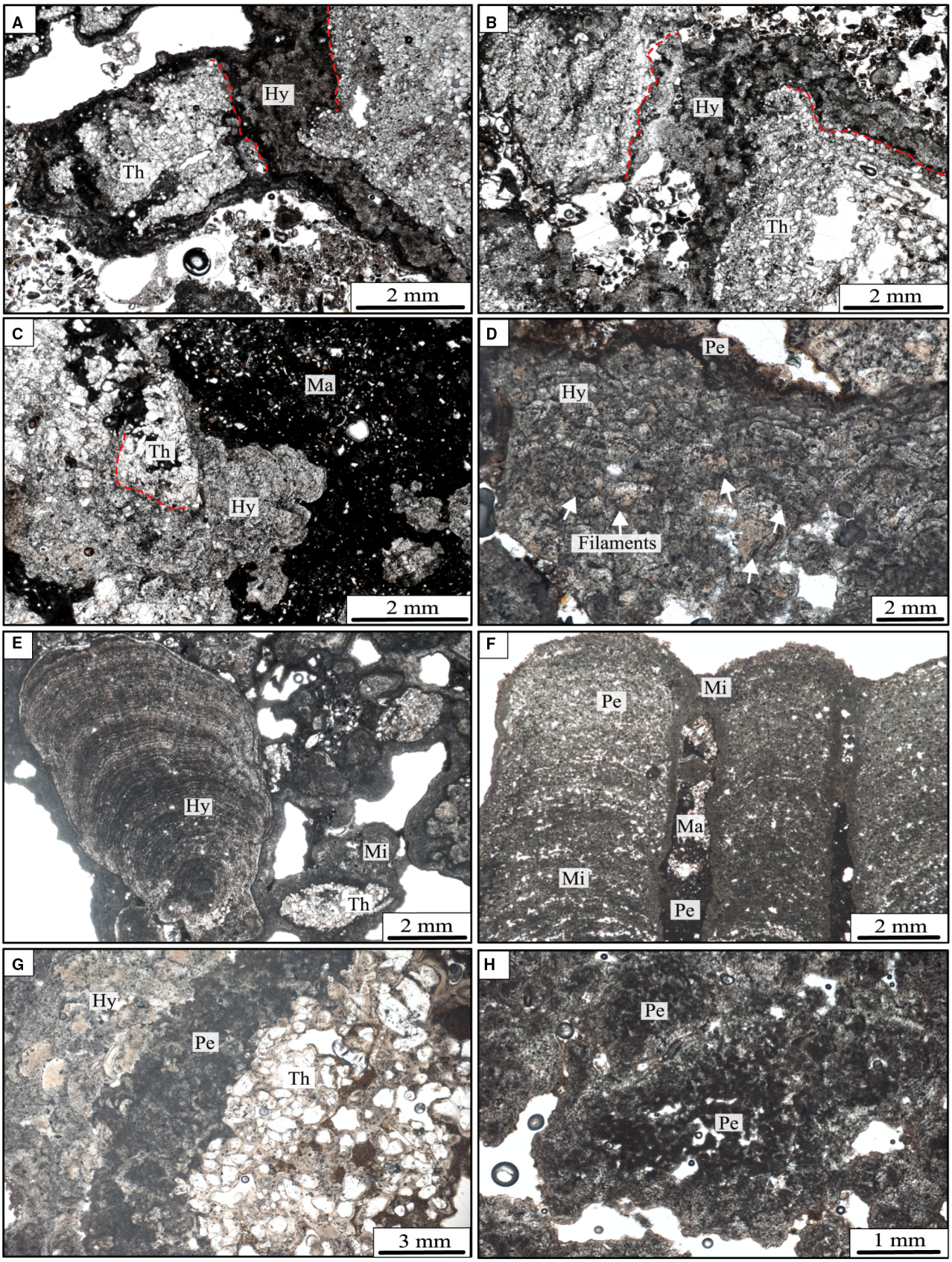

Fig. 9. Microstructures of the carbonate buildups of the Winnemucca Lake and Pyramid Lake. (A) and (B) Thinolites (Th) preserved as a prismatic crystal shape made of calcite, encrusted by microbialites [organized as hybrid (Hy) microstructures composed of alternating large crystals and micrite]. (C) Thinolites (Th) encrusted by a hybrid microstructure (Hy) of possible microbial origin embedded in a micritic matrix (Ma; matrix of wackestone with ostracodes and floating crystal of thinolites). (D) Microbialites with a hybrid microstructure made up of fan-shaped calcite crystals and micritic layers (Hy) including microbial filaments (white arrows). (E) Columnar microbial structures with a hybrid microstructure made of cements and micrite and pseudomorphs of thinolite, encrusted by irregular laminated micritic layers (Mi). (F) Microbial-rich columns made of peloids (Pe) and micrite (Mi), growing vertically and embedded in a micritic-rich (Ma) matrix with ostracodes. (G) Transition from thinolites (Th) pseudomorphs, to encrusting peloidal (Pe) microbial crusts and hybrid (Hy; highly cemented) microbial (?) layer. (H) Peloids (Pe) organized in clusters, producing a clotted mesostructure.

Drakos & Faulds, 2013). The south-western area comprises andesites, breccia and pyroclastic rocks. All of the basaltic rocks are poorly altered (Fig. 14A). The eastern flank of the sub-basin is characterized by a more diverse lithology with rhyolites in the southern part and shales to granodiorites increasingly present towards the north (Fig. 14C and 14D). Except for the rhyolites, all lithologies are strongly altered with arenite covering the granodiorites and silt covering the metamorphic shales (Fig. 14A). Some spurs of rhyolitic breccia are covered by a microbial matrix encrusting blocks and pebbles (Fig. 14D and 14G). The rhyolites are cross-cut by dykes that form cohesive and resistant structures on the lake bottom. The lithological distribution is less diverse in the Pyramid Lake watershed (Fig. 11B), where basalts, andesites and dacites make up the northern three quarters of the lake. As is the case for Winnemucca sub-basin, these formations are well-preserved. The southern flank has a more diverse lithology with well-preserved rhyolites, basalts and highly altered granodiorites cropping out mainly in the south-western part of the lake.

Sedimentary lacustrine substrates

Clastic and carbonate deposits are the two main lithologies making up the sedimentary substrate of the lakes. The clastic deposits are mainly fine-grained sediments at the bottom of the lake and coarser conglomerates and blocks (Fig. 14E to H) forming lake terraces, debris flows and occasionally deltaic lobes (Blair, 1999). Conglomerates are frequently found upslope or at the base of the large complex domes, where they fill in dissolution cavities or wrap around buildups and are observed on terraces inclined towards the lake depocentre (Fig. 14G). Similar to Lake Bonneville, microbial peloidal cements commonly seal and stabilize the flat conglomerates on horizontal terraces and in debris flows along the slope that borders terraces and deltaic lobes (Vennin *et al.*, 2019). The carbonate substrate consists of previously formed microbial-rich buildups and thinolites (Fig. 5C to E and 14F).

INTERPRETATION AND DISCUSSION

Depositional processes for the buildups

The lakes in the west and east of the Great Basin accommodate an important diversity of carbonate buildups with respect to size, shape and distribution. Based on the literature at the Great Basin scale (Brasier *et al.*, 2018; Vennin *et al.*, 2019; DeMott & Scholz, 2020) and microscopic information provided in Table 1, buildups are interpreted as a hybrid of chemically-induced and biologically-induced carbonates.

In contrast to the buildups in Lake Bonneville and Great Salt Lake which comprise microbialites (Pace *et al.*, 2016; Bouton *et al.*, 2016a,b; Vennin *et al.*, 2019), the complex domes and the thinolite-rich hemispheroid domes in the western Lahontan lacustrine system are hybrid carbonates (Fig. 9). These carbonates are composed of acicular crystals of calcite (thinolites; Fig. 9A to C) formed by abiotic precipitation (Shearman *et al.*, 1989; Trampe *et al.*, 2016). They are encrusted by dark micritic laminae, including filaments and diffuse peloids or hybrid microstructures that consist of cements/filaments or peloids/cements. These crusts are interpreted as microbial-induced precipitation similar to crusts described for microbialites in Lake Bonneville (Vennin *et al.*, 2019), Great Salt Lake (Thompson *et al.*, 1990; Chafetz & Buczynski, 1992; Pace *et al.*, 2016; DeMott *et al.*, 2019a, b; Lindsay *et al.*, 2020; Cohen, 2021) and Mono Lake (Brasier *et al.*, 2018). The capping crusts, microbial-rich hemispheroid domes and the columns are mainly composed of microfabrics dominated by filamentous microorganisms (Fig. 9D), micritic laminae (Fig. 9E), diffuse peloids

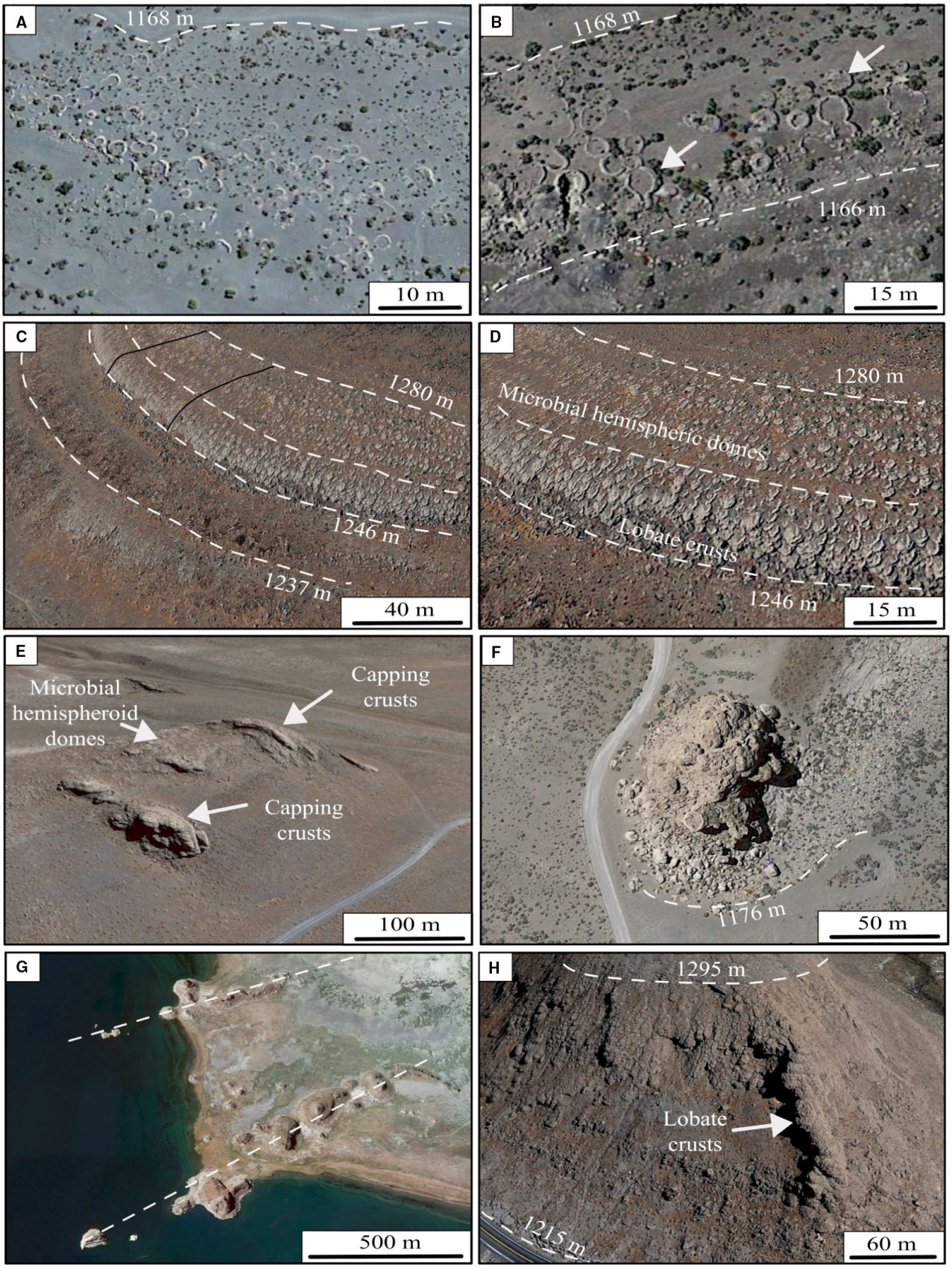

Fig. 10. Aerial view of the carbonate structures mapped using Google Earth Pro software (V7.3.4.8248–16 July 2021, Nevada, USA. © 2021 Google). For location of all the images see Fig. 1C. (A) and (B) Thinolite-rich hemispheric domes distributed along the shores of Winnemucca Dry Lake between 1158 masl and 1180 masl. (B) Domes distributed along a beach ranging from 1166 to 1168 masl. Eroded hemispheroids exhibit a ring shape (white arrows). (C) and (D) Capping crusts and microbial domes arranged along shoreline ranging from 1246 to 1280 masl; (D) is a close-up view of a terrace depicted in (C) and shows the organization of small structures according to the slope gradient. The crust morphologies evolve from microbial hemispheroid domes in very flat slope along the shore to lobate capping crusts when slope increases. (E) Encrusted rocky promontory on the eastern shore of Pyramid Lake; microbial hemispheric domes are observed in flat area of the shore and capping crusts where the slope increases. (F) Isolated dome and barrel complex structures. (G) Aerial view of the Needle Rocks columns aligned along faults (North Pyramid Lake; white dashed lines). (H) Lobate crusts encrust the promontory of Marble Bluff on the south-eastern shore of Pyramid Lake. Crusts seem to flow over the substrate (top to bottom vertical growth).

organized in clotted fabric (Fig. 9H) or centimetre-high columns (Fig. 9F). Peloids can be distinguished from well-rounded faecal pellets by a smaller size and a diffuse contour. Despite a possible biotic and/or abiotic composition of the peloidal cements, their proximity to thin filaments suggests a microbial origin.

External parameters controlling development of buildups

Substrate controls on microbial-rich carbonate distribution

Based on the mapping of the buildups, substrate lithology seems to be a dominant factor controlling microbialite development and preservation. When substrates are loose and dominated by fine-grained sediments (i.e. altered granodiorites, shales and lacustrine fine-grained sediments), no microbialites develop. Typically, cohesive, firm and stable substrates are favoured over soft substrates to support formation of microbial carbonate deposits (Bouton *et al.*, 2016b; Roche *et al.*, 2019; Vennin *et al.*, 2019). The solid substrates allow a more rapid and extensive settlement of the microbial mats (Pedley, 2014; Roche *et al.*, 2019). Weakly altered basalts, andesites, dacites and rhyolites present at various elevations are often covered by thin (centimetre-thick) to thick (decimetre to metre-thick) microbial carbonate crusts (Figs 4, 11 and 14A to C). The rhyolitic spurs composed of breccia and the dykes observed the lake bottom can also support the development of the microbial crusts and domes (Fig. 14A). On both sides of the Great Basin, coarse-grained lacustrine sediments, such as conglomerate debris flows, and isolated erratic blocs are frequently covered by microbial crusts and associated with centimetre-high columns (Fig. 14G and H). The distribution of the carbonate buildups can also be driven by the presence of lobe-shape conglomerates and terrace, where the conglomerates act as stable nucleation points. In the Winnemucca Lake, pipe-like columns protrude through a clast-supported conglomerate and lacustrine sediments (Fig. 14H). Their formation results from groundwater circulation (Fig. 15) and are considered as venting fluid pipes by DeMott & Scholz (2020). These pipes are characterized by the development of clotted and laminated mesofabrics related to biologically-induced processes.

In the Lahontan sub-basins, the substrate lithology and cohesiveness can explain some of the contrasting distribution of microbial buildups in the east (dominated by strongly altered rocks) and the west (dominated by poorly altered basalts), which preferentially establish on firm and stable substrate. In addition to providing a physical support for microbialite development, the substrates, when altered, contribute to ions necessary for mineralization (Chafetz *et al.*, 1991; Gradziński, 2010; Roche *et al.*, 2018). The buildups composed of thinolites are the only ones that develop at the interface of soft sediment and water, because they are composed of acicular crystals lacking trapped siliciclastic material (Council & Bennett, 1993; Huggett *et al.*, 2005). Importantly, the substrate lithology and the granulometry determine the presence and distribution of buildups, however, not their morphology.

Physiographical controls on carbonate morphologies

Physiography is another important controlling factor, which affects the development and distribution of buildups on the shore of both Pyramid and Winnemucca sub-basins. On the eastern side of the Great Basin, Lake Bonneville is dominated by successive, vertically-growing narrow belts on the edge of the deep lake. The basin structure is largely shaped by the tectonics which directed the subsidence (Bouton

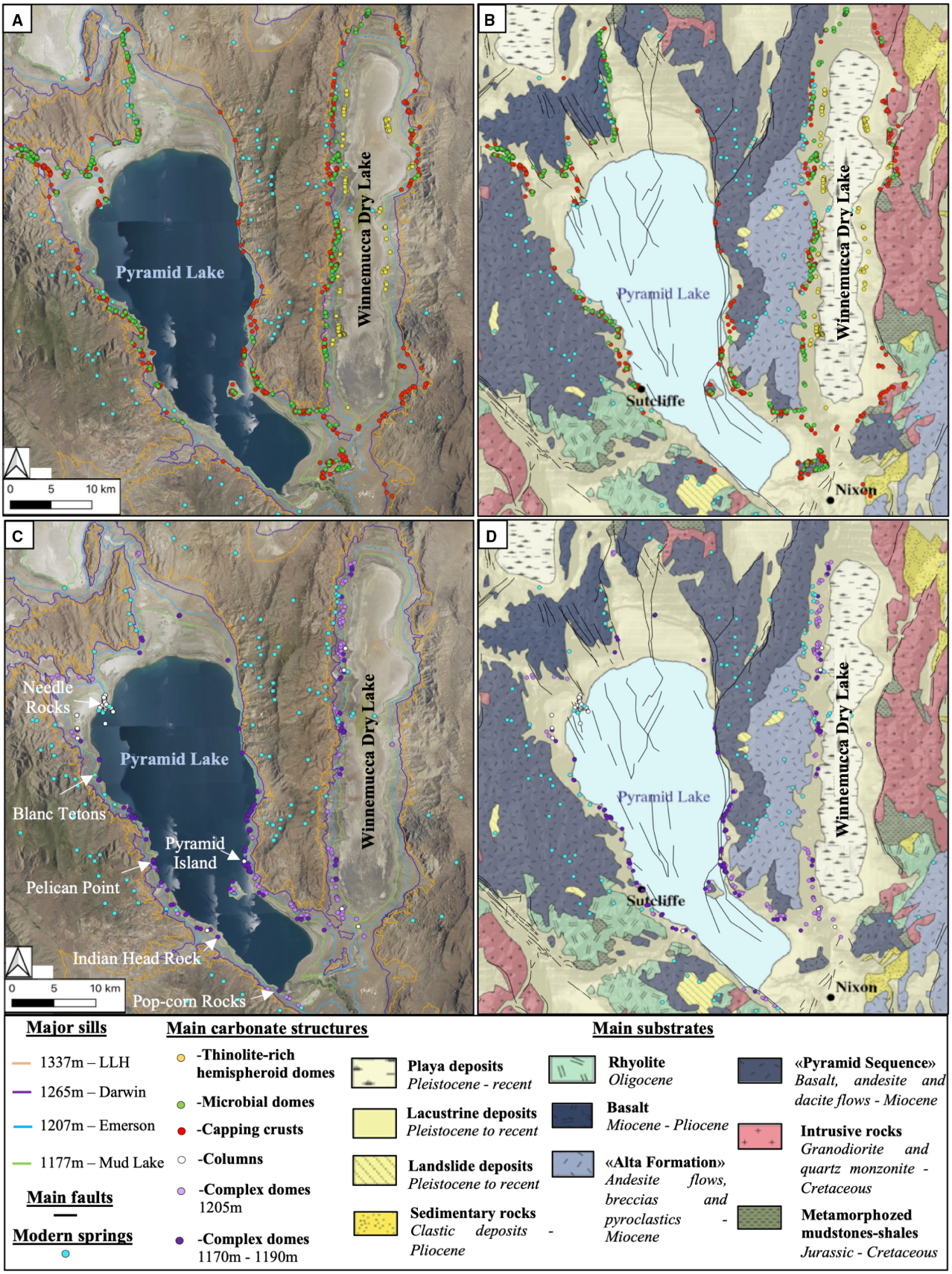

Fig. 11. Small-scale carbonate macrofabrics (A and B; thinolite-rich hemispheroid domes, microbial hemispheroid domes and capping crusts) and the large-scale carbonate macrofabrics (C and D; complex domes and columns) on the shore of both Pyramid and Winnemucca sub-basins. Representation of the small-scale macrofabrics (A) and large-scale macrofabrics (C) in relation to the major elevation sills located according to Benson *et al.* (2013a,b) and Adams & Rhodes (2019). The map depicted an aerial view of the study area (NAIP 2019; www.earthexplorer.usgs.gov). Small-scale (B) and large-scale (D) macrofabrics on Pyramid and Winnemucca sub-basins superimposed on the geological map background, modified from Nevada Geologic Units GIS data, Stewart *et al.* (1982); Washoe and Storey Counties geological map, Bonham Jr. (1969); and Sahwave and Nightingale Ranges Van Buer (2012). The fault mapping (black lines) is based on seismic data of Anderson *et al.* (2013) and Eisses *et al.* (2015). The modern springs (blue points) are mapped according to their visibility on Google Earth Pro (V7.3.4.8248, Nevada, USA. © 2021 Google).

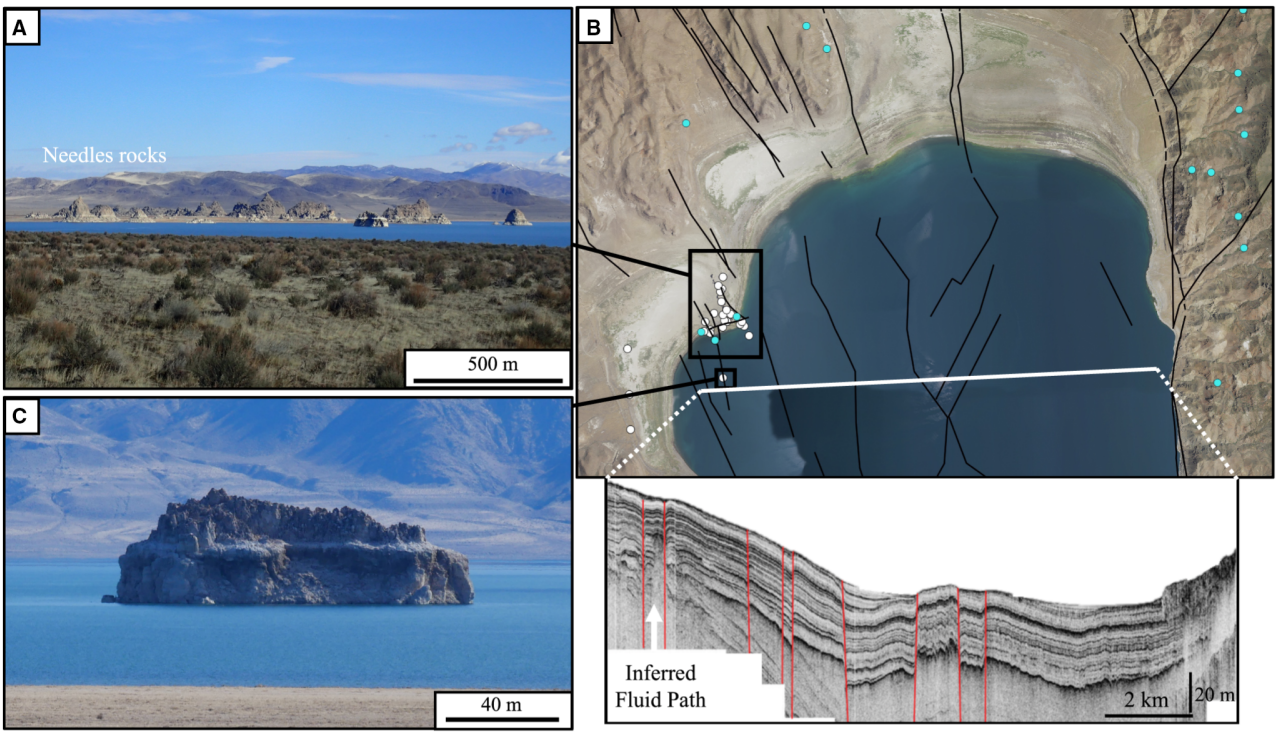

Fig. 12. Relationship between the location of faults and the distribution of the large carbonate buildups of Needle Rocks. (A) Alignment of the Needle Rocks columns along the faults (white dashed lines), north-east of Pyramid Lake. (B) Evidence of the columns (white dots) and faults (black dashed lines) relationship in an aerial view. The white line shows the location of a seismic profile obtained by Eisses *et al.* (2015) during a campaign in 2013, with red lines showing the location of faults in the subsurface. (C) Carbonate buildups forming an island occurring in the lake, positioned along the Needle Rocks columns, near a fluid resurgence and overlying a fault.

et al., 2016a,b). As discussed by Vennin *et al.* (2019), despite a predominantly climatic control on the distribution of microbial buildups, aligned faults and local topographical structures play a role on their morphology (see fig. 12 in Vennin *et al.*, 2019).

This specific tectonic mechanism can also be proposed for the Lahontan lacustrine system, where the sub-basins are shaped by the tectonic framework of the Great Basin with steep faults, inducing scarps in the topography (Smith & Bruhn, 1984). In the extensional half-graben Lahontan sub-basins, the steep slopes are formed by normal faults, which are particularly common at the eastern edges of the sub-basins and result in an asymmetrical basin (DeMott & Scholz, 2020). This particular geomorphology explains, in part, the east/west asymmetrical distribution of various buildups, that increase in abundance along the western side of the lakes

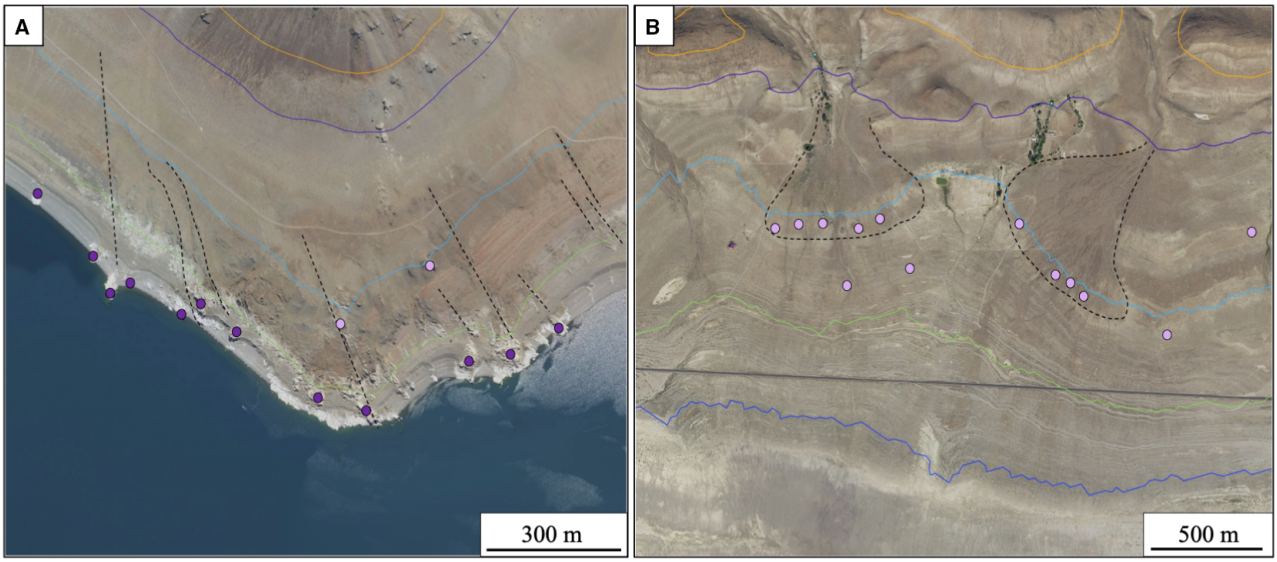

Fig. 13. Complex dome structure distribution on the shores of Pyramid Lake and Winnemucca Lake. The dark purple points indicate the location of domes between 1170 masl and 1190 masl. The light purple points indicate the location of domes mainly occurring at 1205 masl elevation. (A) Complex domes located near faults (black dashed line) on the western shore of Pyramid Lake. (B) Complex domes located in the outskirts of fossil deltaic fan-shaped structures (black dashed line) on the shore of Winnemucca Dry Lake. The coloured lines represent the level of the main terraces (green line: Mud Lake sill, blue line: Emerson sill, purple line: Darwin sill and orange line: Lake Lahontan high stand) according to Benson *et al.* (2013a,b) and Adams & Rhodes (2019). The contemporary prings (blue points) are mapped according to their visibility on Google Earth Pro (V7.3.4.8248 (16 July 2021) Nevada, USA. © 2021 Google).

(Fig. 11). On the banks of both Pyramid Lake and Winnemucca Lake, the steepness of slopes increases with increasing elevation. Typically, the areas with the gentle slopes (<10°) are confined to the lower levels of the watershed, and the higher elevations are marked by slopes of up to 90°, except on terraces. The slope directly affects the shape and location of buildups: on higher elevations, from 1174 to 1330 masl with the steep slopes (above 30°), only capping crusts are found. Similar slopes are present on banks and edges of rocky spurs, where only crusts occur (Fig. 16A). The slope also impacts morphology of buildups (Fig. 4): on the steepest slopes that are almost vertical, the capping crusts form either drapes or "bird's-nest" structures, which overlap one another (Fig. 4B and C). Where the slope slightly decreases (between 10° to 30°), the crusts are more lobate and 'flow' over the substrate (Figs 4A and 10H). This 'flowing' appearance is similar for the lobate crusts that form below the terraces and on multi-metre sized columns and complex domes (Fig. 6A to C). On gentle to moderate slopes (<10°) and flat terrace surfaces, the microbialites establish hemispheroid domes that align in belts along the shorelines (Fig. 10C and 10D). Thus, the changes in morphology of the carbonate buildups are strongly correlated with the slope determined by the inherited physiography (Fig. 16A).

Fig. 14. Nature of the different substrates and their role on the development of buildups (see Fig. 1C for location). (A) Planar capping crust developed on a vertical basaltic wall. (B) Detail of a large development of planar and lobate capping crusts upon a rhyolitic substrate. (C) Poorly-developed carbonate crusts upon altered granodiorite, producing arenite. (D) Capping crusts developed upon mineralized faults in the front. No crusts are observed on the metamorphized mudstone-shales in the back. (E) Capping crusts and hemispheroid microbial domes developed upon conglomerate in the Winnemucca Dry Lake. (F) Draping planar capping crusts develop upon a columnar carbonate substrate (interpreted as a chimney). (G) Encrusting microbial crust developed on rhyolitic breccia forming a spur on the lake bottom. The spur is covered by a complex microbial dome. (H) Small-scale (circular-pipe) columns cross-cutting the conglomerates and organized as coalescent structures.

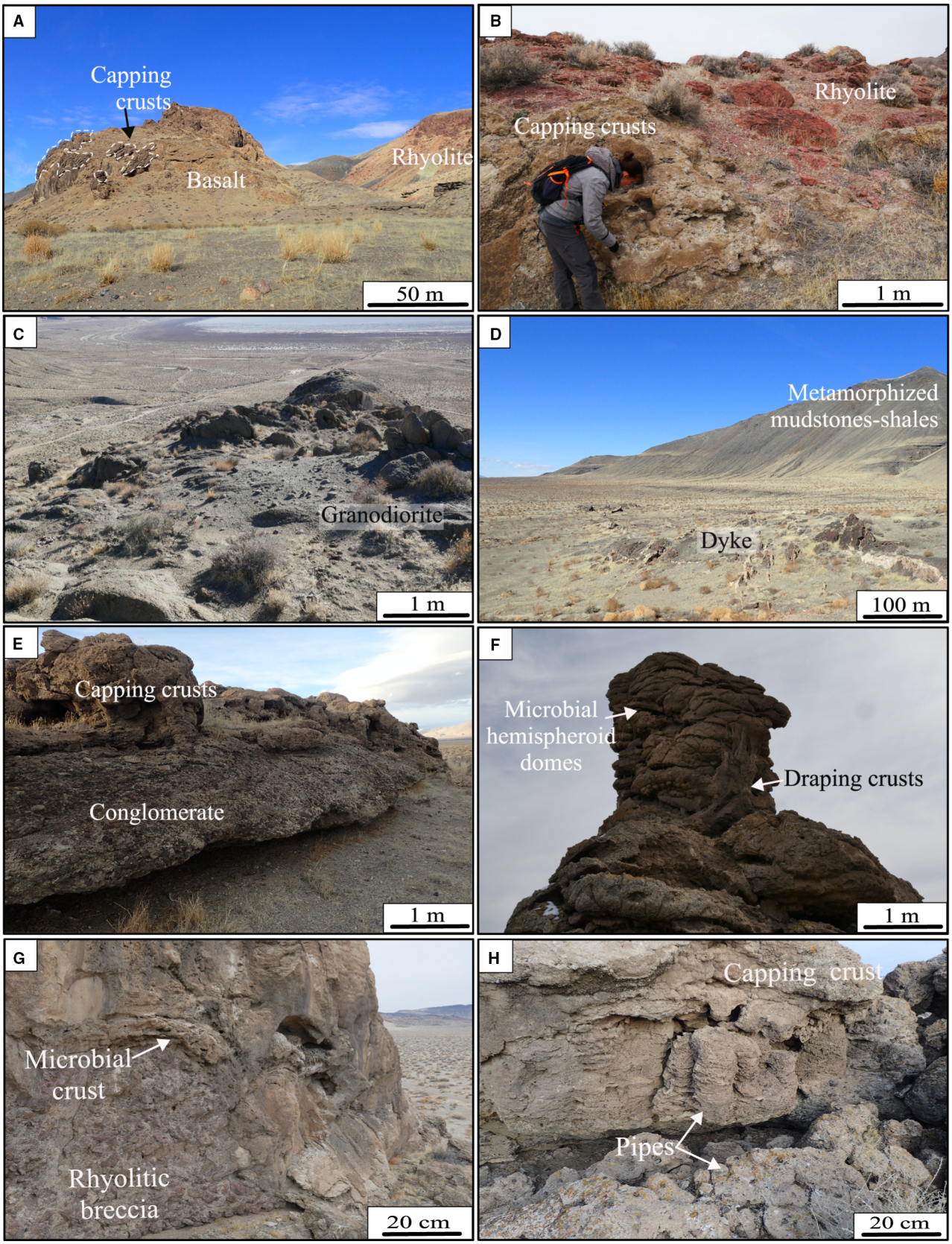

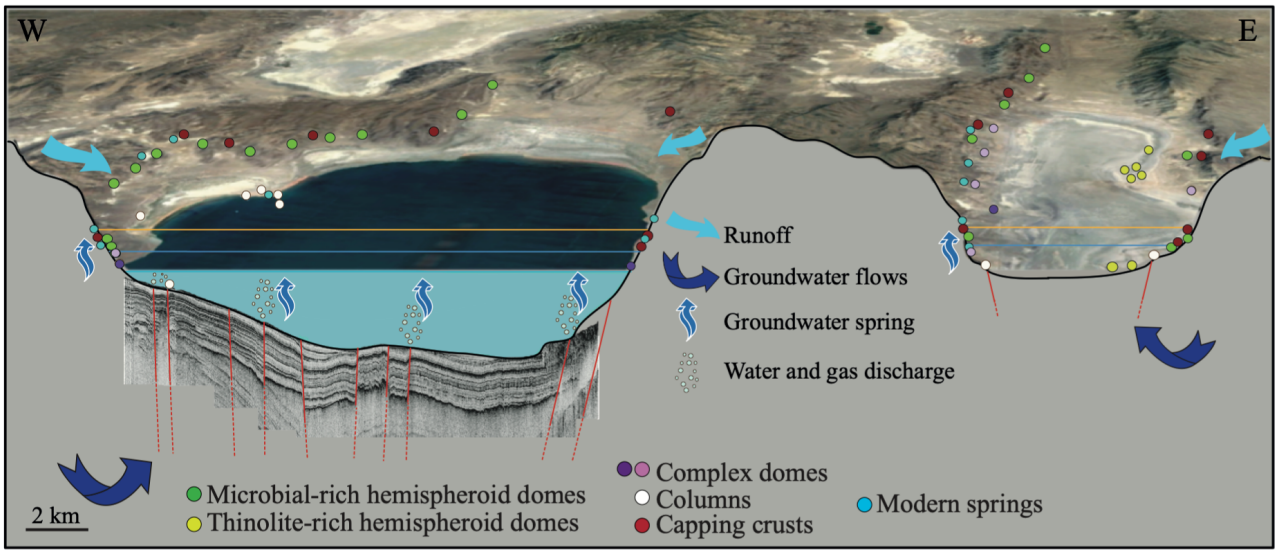

Fig. 15. Model of different fluid inputs along faults and springs associated with groundwater recharges and runoff or surface flow; the microbial-rich structures are distributed close to the springs, along the faults and the shore of the lake. Integration of seismic profile obtained by Eisses *et al.* (2015) during a campaign in 2013 and a topographical profile from Google Earth (V7.3.4.8248, Nevada, USA. © 2021; X2 vertical exaggeration).

Accommodation space control of carbonate structure distribution

Figure 16 summarizes changes in water elevation and the distribution of the different carbonate buildups. The size and morphology of the carbonate buildups are also controlled by the accommodation space and fluctuation in the base level depending on climate and tectonics (Della Porta, 2015; Bouton *et al.*, 2016a,b). The distribution of carbonate buildups is also determined by the water depth and typically follows the shoreline (Figs 11, 15 and 16). Microbially-mediated precipitation, shown by stable isotope and organic geochemical evidence (DeMott & Scholz, 2020; this study), is a biotic control which potentially dictates the buildup development. Oxygenic photosynthesis is a key metabolism in microbialite development, which suggests another potential control on buildup development, such as the light availability and nutrients (Visscher *et al.*, 2022). Photosynthetic CO_2 fixation enhances the nucleation of carbonate minerals by fixing CO_2 and increasing pH (Visscher *et al.*, 1998; Dupraz *et al.*, 2009; Arp *et al.*, 2012). Changes in water depth can control the light available for photosynthesis.

When the water level fluctuates, predominantly thin microbial crusts form on vertical walls (Vennin *et al.*, 2019). The planar and lobate crust morphologies thus likely indicate increase or decrease in water level. The planar capping crusts (Fig. 4C to E), with 1330 masl as the upper limit of distribution, line the cliff wall when the lake level recedes. The lobate "bird's-nest" structures frequently develop on the planar crusts, indicating a subsequent increase in water level until a platform was reached (Fig. 4B and 4C). The development of these platforms ultimately reached the elevation of a terrace, in this case to the level of the Darwin sill.

Fig. 16. Illustration summarizing the distribution of the main carbonate structures (see Table 1 for detailed description) on the shores of the Lahontan: Pyramid–Winnemucca (A) and Bonneville and GSL (B) lakes. The distribution of the carbonate deposits is juxtaposed with the elevation of the main terraces and associated with the evolution of the water level since 30 kyr cal BP; the colour of the carbonate structures corresponds to the colour used for mapping (Figs 11 and 13). (A) The lake level curve (blue curve) and the elevation of the terraces are based on Adams & Rhodes (2019) and Benson *et al.* (2013b); the box plots show the slope interval for each structure (CC: capping crust, C: column, CD: complex dome, MHD: microbial hemispheroid dome, THD: thinolite-rich hemispheroid dome). (B) The lake level curve (blue) and the elevation of the terraces are based on Oviatt (1997, 2015), Murchison (1989), Patrickson *et al.* (2010) and Vennin *et al.* (2019).

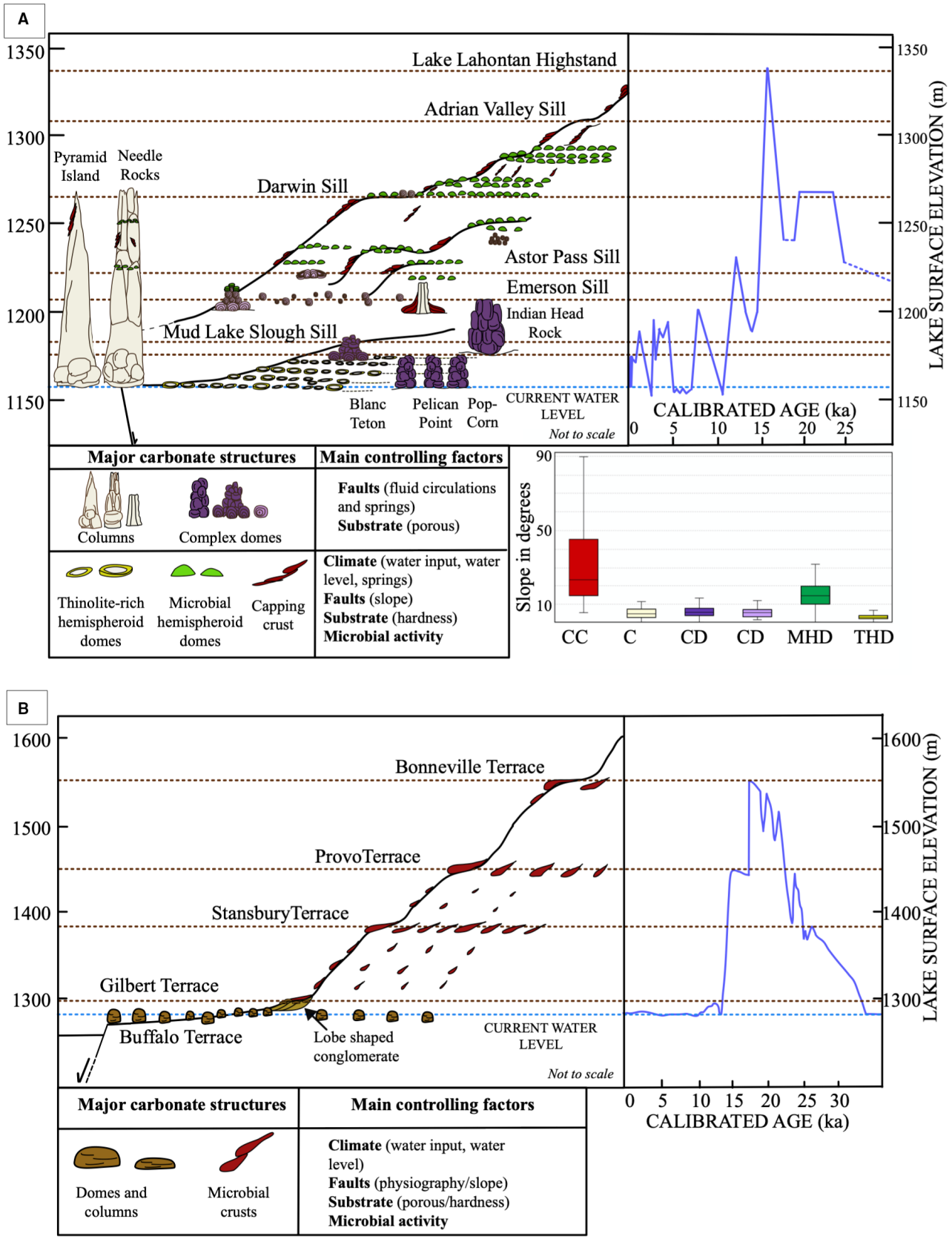

During periods of lake level stabilization microbial-rich hemispheroids developed as belts along the shore and grew following a progressive increase in accommodation (Fig. 16A). The presence of comparable small-scale hemispheroid domes in both lakes, at the same elevations (from the Astor Pass sill to just below the Adrian Valley sill) suggests a connection between the two sub-basins, at least until they were isolated by the Mud Lake Slough sill (1177–1183 masl) about 3 ka (Fig. 11A and 11B; Adams & Rhodes, 2019). The presence of more buildups in the sills than in terraces may be related to increasingly severe hydrodynamic conditions in narrow areas (Pedley, 2000; Arenas-Abad *et al.*, 2010; Roche *et al.*, 2019). Ring-like hemispheroids have preferentially been preserved along palaeoshorelines and are believed to require some degree of exposure and recurrent emersions (Bouton *et al.*, 2016b; Vanden Berg, 2019). The taller hemispheroid domes are preserved better and most likely developed deeper in the sublittoral zone characterized by higher accommodation space. These largest hemispheroids grow on flooded topographic highs (for example, spurs and deltas). The upper limit of the water level elevation can be estimated from the maximum vertical development of the buildups, until the formation of an erosion or emersion surface, i.e. when the buildups reach the water surface (Bouton *et al.*, 2016a,b; Roche *et al.*, 2018; Vennin *et al.*, 2019, 2021). A similar distribution of the hemispheroids and crusts is found along the shorelines of the Bonneville and GSL phases (Fig. 16B; Bouton *et al.*, 2016b; Vanden Berg, 2019; Vennin *et al.*, 2019). The larger sublittoral microbial bioherms mainly developed on topographic relief in the eastern Great Basin (Baskin *et al.*, 2021). In the Lahontan sub-basins, the tallest buildups (columns and complex domes) require a high accommodation space and follow an increase in water elevation up to the Darwin sill as proposed by Benson (1994).

Large-scale carbonate structures link with groundwater circulations and faults

The columns and complex domes are the largest carbonate buildups in both Pyramid and Winnemucca sub-basins. They are absent in the eastern Great Basin (Fig. 16A and 16B), where only capping crusts and peloidal cements formed in narrow belts on the terraces and vertical cliff walls of Lake Bonneville. The largest microbialites that developed during the GSL phase are the metre-thick columns in the distal part of the lake (Fig. 8E to H; Bouton *et al.*, 2016b; Vanden Berg, 2019; Vennin *et al.*, 2019; Baskin *et al.*, 2021). In the Lahontan lacustrine system, columns are generally found at low elevation, associated with soft lacustrine sediments, and do not grow along the palaeoshorelines. The complex domes are often found along shorelines and aligned with the lake flanks. Both types of buildups in the two sub-basins are associated with normal faults (Figs 10G, 11C, 11D, 12A and 14). The column alignments strictly overlap with faults, but in contrast, the distribution of complex domes is restricted to faults or linked to springs (Fig. 13A and 13B).

Fluid circulation evidence and current groundwater springs

The juxtaposition of faults and buildups has motivated speculation that tectonics plays a role in the mineralization processes and, consequently, consider these structures as groundwater-related carbonates (Benson *et al.*, 1995; DeMott *et al.*, 2019b). Similar to Lake Abhé (Dekov *et al.*, 2014), Lake Afdera (Schaegis *et al.*, 2021) and Mono Lake (Brasier *et al.*, 2018), the faults may enable the upward circulation of fluids to the surface and form large structures (Benson, 1994; DeMott *et al.*, 2019b; DeMott & Scholz, 2020). The local groundwater resurgences support the construction of large buildups, and when the flow is diffuse, it favours the formation of smaller structures that are spread out over larger areas (Benson *et al.*, 1995; Forrest & Melwani, 2003; Prol-Ledesma *et al.*, 2004; Forrest *et al.*, 2005; DeMott *et al.*, 2019b; DeMott & Scholz, 2020). However, even if a link between faults and the carbonate production could exist, no robust evidence for this has been found in the Pyramid and Winnemucca sub-basins. In the former sub-basin, Benson *et al.* (1995) and Benson (1994) showed that the large carbonate constructions are systematically associated with springs along the shore. Some complex columnar and dome structures thrive where contemporary springs discharge cold (Popcorn Rocks; Coolbaugh *et al.*, 2009), or hot (Needle Rocks; Arp *et al.*, 1999 and Pyramid Rocks; Coolbaugh *et al.*, 2009), waters or are associated with deep hydrothermal systems that are not visible (Astor Pass; Vice *et al.*, 2007).

The large carbonate structures of both Winnemucca and Pyramid sub-basins often have

small-scale pipes in complex domes as well as at the core of columns (Fig. 6). Theses pipes are interpreted as fluid circulation conduits for spring discharge (Coolbaugh *et al.*, 2009). This allows Ca^{2+} rich fluids to mix with the lake water, causing localized supersaturation of carbonates that could result in mineralization (Benson *et al.*, 1995; this study, Table 2). The growth of the carbonate buildups is thus vertical and could account for the large size of some of the columnar structures. As long as the columnar structures are submerged, the mineralization, and thus the growth, of these structures is supported. In contrast, when the lake level is lower than the highest part of the structure, the mixing zone cannot form and vertical expansion of the column ceases. The limited available dating (Benson *et al.*, 2013b; DeMott *et al.*, 2019b) suggests that mineralization occurs during the period of lake level rise (starting at 45 kyr cal BP) as well as during periods of highstands (until 15 kyr cal BP, Figs 2 and 16A). Estimates for the age of the Needle Rocks columns indicate that the development of these structures progressed as the lake level rose, until the maximum height of 1270 masl was reached. The stabilization of the water level in the lake, marked by the Darwin sill at 1265 masl, likely impeded further chimney growth (Fig. 16A). The dating of the barrel-shaped structures at Blanc Tetons, Pelican Point and Popcorn Rocks (Benson *et al.*, 1995), and their relation to the water level curve (Fig. 2), indicates that these large-scale buildups formed when the water level was high. In addition, numerous smaller structures with internal pipes were found in conglomerate deposits and in deltaic sediments (Fig. 14H). The development of these features is the result of water discharges through porous sediments, supported through a fossil circulation system. In Winnemucca Lake, the tall columns occur less frequently and are aligned along blind faults parallel to the visible fault pattern. Regardless of the mode of circulation, groundwater flow coincides with deep normal faults (Vice *et al.*, 2007; Kratt *et al.*, 2010; Dekov *et al.*, 2014; Cukur *et al.*, 2015). Accordingly, tectonic processes are required to produce the large carbonate structures (Vice *et al.*, 2007; DeMott *et al.*, 2019b), a scenario which is supported by seismic and mineralogical observations (Fig. 12).

Table 2. Physico-chemical composition of the Great Salt Lake (GSL): lake, tributaries, springs and Pyramid Lake: lake, river, hot and cold springs.

			Mean $[Ca^{2+}]$ ($mg{\cdot}L^{-1}$)	Water flow ($km^3{\cdot}yr^{-1}$)	References
Bonneville lacustrine system	**Great Salt Lake**		300	–	Bouton *et al.* (2020)
		Rivers			
		Weber River	61.62	1.28	
		Bear River	64.24	2.44	
		Jordan River	112.47	1.39	
		Springs Average	271.4	–	
Lahontan lacustrine system	**Pyramid Lake**		8.42	–	Visher (1957); Benson and Leach (1979); Benson (1994); Benson *et al.* (1996); Mohammad and Tempel (2019)
		Rivers			
		Carson	10	0.454	
		Humboldt	38	1.009	
		Quinn	30	0.036	
		Susan	10	0.085	
		Truckee	8.82	0.725	
		Walker	34.4	0.379	
		Hot springs			
		Needles spring	172.3	0.0002	
		Needle Well	228.4	–	
		Cold springs			
		Popcorn Rock	8.4	–	
		Pelican Point	3.2	–	

Seismic and chemical evidence of the influence of faults and springs on carbonates distribution and fabrics.. Tectonic activity and faulting have been studied more extensively in Pyramid Lake than in the other lakes of the Lahontan lacustrine system. In part due to geothermal surveys, the location of faults is particularly well-documented in Lake Pyramid (Figs 11B, 11D and 15; Coolbaugh *et al.*, 2007, 2009, 2010). Data in Eisses *et al.* (2015) for Pyramid Lake showed numerous north/south trending normal faults with fluid circulation, both along the shoreline and across the lake. When superimposed on the maps of carbonate structures, these faults show a correlation of the large-scale deposits with geodynamic activity. A clear relationship between faults and the distal carbonate structures of Needle Rocks could be identified along line D01L01 (Eisses *et al.*, 2015; Figs 12 and 17). However, the origin and composition of the fluids (i.e. groundwater recharge versus a hydrothermal input) that have percolated through this fault system is unknown. The numerous gas pockets in the seismic data of Pyramid Lake were presumably produced by microbial degradation of organic matter (Eisses *et al.*, 2015). It is possible that these gases diffuse upward through the sediments or vent through a fault network and enhance carbonate precipitation.

In the Winnemucca sub-basin, the presence of columns is usually associated with faults, but the distribution of complex domes, which dominate the flexural margin of the half graben, is not. These buildups occur at two specific elevations (around 1170 to 1190 masl: dark purple circles on Fig. 11; and 1195 to 1220 masl: light purple circles), where they are associated with springs and aligned in front of fan-deltas that support a specific groundwater flow path. The springs are constrained between bedrock and the alluvial deposits (mean elevation approximately 1270 masl) in the western margin and favour the direct fluid path. In the eastern margin, the presence of the springs at higher elevation (1300 masl and upward), above bedrock/alluvial limit, does not support a specific fluid path. DeMott & Scholz (2020) propose a comparable diffusion, along stratigraphically-controlled groundwater flow path as a driver for the development of some buildups (Figs 13B and 17). This scenario is applied to both south-eastern and western margins of Pyramid Lake where the complex domes develop on spring-related faults and in front of a delta (Fig. 13B). The development of complex domes is similar to that of crusts and hemispheroids and coincides with a period of stillstand corresponding to the elevation of Mud Lake and Emerson sills, respectively. In contrast to the small-scale buildups, formation of complex domes coincides with spring groundwater discharges and develop on or close to terraces. During the Bonneville and GSL phases, deltas mainly offer a substrate for microbialite development, especially that of crusts and microbial hemispheroid domes (Fig. 16B).

A mass balance approach (Bouton *et al.*, 2020) showed that the amount of carbonate precipitation in GSL depends on the Ca^{2+} input by the combined tributaries. As proposed by Richardson (1906) and Bouton *et al.* (2020), the low concentration of Ca^{2+} in the water column of the lake does not explain the large amount of calcium carbonate stored in the sediments. This implies that the residence time of the ions in the water column is short and precipitation of $CaCO_3$ or, alternatively, scavenging by EPS (Dupraz & Visscher, 2005) take place rapidly. Bouton *et al.* (2020) estimated that a similar amount of calcium was delivered by the rivers and was ultimately stored as carbonates in the basin. In Pyramid Lake, the concentration of Ca^{2+} is also very low (8.42 mg l^{-1}) and, as in GSL, does not explain the calcium carbonate stored in the sediments (see Table 2 and Appendixes S1 and S2). In contrast to the GSL tributaries, the delivery of calcium by the Truckee River to Pyramid Lake is very low (Benson & Peterman, 1996; see Table 2 and Appendixes S1 and S2). Estimates for Pyramid Lake and Winnemucca Lake, for the last 10 ka show a deficit of Ca^{2+} between river delivery (approximately 64 Mt) and Ca^{2+} stored in the carbonate sediments (approximately 156 Mt). During the fossil period corresponding to complex dome growth (approximately 10 ka; see Appendix S1), the Lahontan lacustrine system shows a smaller deficit of Ca^{2+} between river delivery (approximately 1.54 Gt) and Ca^{2+} stored in the carbonate sediments (approximately 4.17 Gt). Calculations herein (see Appendixes S1 and S2) show that the ratio of calcium inputs by rivers and calcium stored in sediments are 2.4 and 2.7, respectively, for the modern and fossil period. In contrast to the values proposed by Bouton *et al.* (2020) for the GSL, the Lahontan Lake System records a significant deficit in calcium between river inputs and that stored in

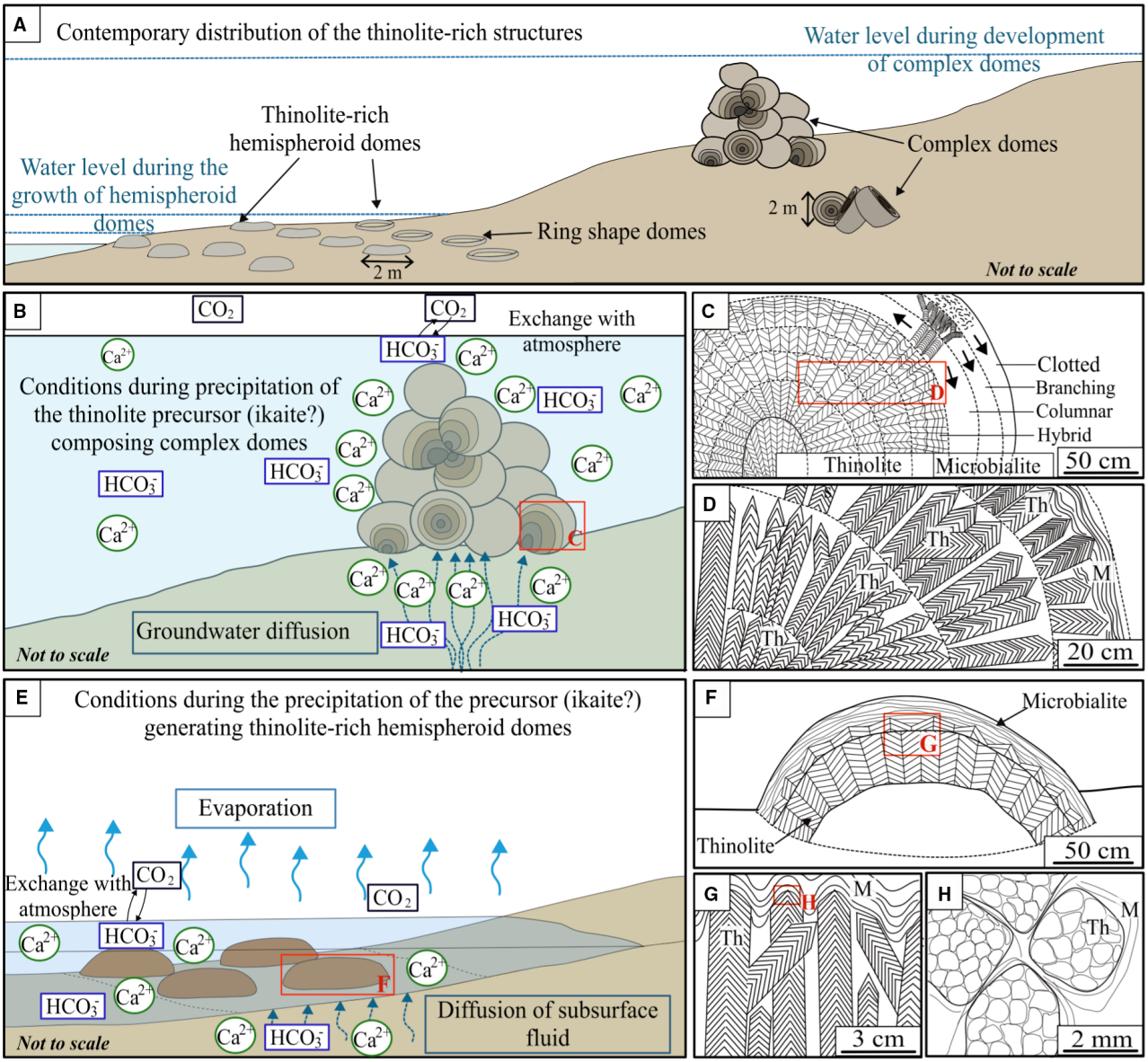

Fig. 17. Model proposed for the formation of thinolite-rich buildups. (A) Contemporary distribution of the thinolite-rich structures in Winnemucca sub-basin. (B) Model showing the conditions during the precipitation of the thinolite precursor (ikaite?) constructing complex domes; close view of the acicular crystal distribution within the domes (C) and (D) and their vertical evolution into microbial-rich layers organized as multi-millimetres thick columns, branches and micrite layers (C). (E) Conditions for precipitation of the precursor (ikaite?) forming thinolite-rich hemispheroid domes under evaporation and close up view of the crystal of thinolite encrusted by microbialites (F). (G) and (H) Detailed views of the microbialite encrusting thinolite composed of scalenohedral calcite crystals replacing a precursor (ikaite?, H).

sediments, especially since these estimates do not take into account the Ca^{2+} stored in buildups. An additional influx of Ca^{2+} that is needed to close the mass budget can be explained by groundwater influxes from hydrothermal and non-hydrothermal sources as proposed by Benson (1994), Matsubara & Howard (2009) and DeMott & Scholz (2020). This sub-surface supply currently accounts for approximately 10% of the total water inputs to the Pyramid Lake sub-basin (Benson, 1994), providing more than two thirds of the total calcium, and may even have been greater in the past. As stated before, groundwater provides ions that upon mixing with lake water can

support carbonate precipitation (Bouton *et al.*, 2020) and form the buildups. The amount of Ca^{2+}stored in the tallest buildups located in the vicinity of faults (i.e. 0.463 Mt in Needle Rocks) is lower than the Ca^{2+} released by the groundwater (*ca* 1.23 Mt) during the time it took for these structures to grow (approximately 30 ka). The excess of Ca^{2+} delivered by groundwater added to the lake water column and could have precipitated as carbonate mud. The absence of large-scale structures in the eastern Great Basin (GSL phase) could therefore be explained by a lower subsurface water flow estimated, contributing only 2 to 3% of the total water input (Hahl & Langford, 1964). The Ca^{2+} availability appears to be the limiting factor for the carbonate precipitation, whether transported by surface streams as in the GSL, or by large groundwater influxes as in Pyramid Lake.

Mineralogical evidence for groundwater circulation. The authors argue that the particular mineralogy of the Lahontan lacustrine system results from specific fluid circulation patterns and fault distribution. Thinolite is one of the major components of calcite in large-scale structures in both Pyramid and Winnemucca sub-basins but is absent in the eastern Great Basin. This crystalline phase is considered to form calcite pseudomorphs after ikaite (Shearman *et al.*, 1989; Bischoff *et al.*, 1993a; Ludwig *et al.*, 2006; Bates *et al.*, 2010; Zhou *et al.*, 2015; Purgstaller *et al.*, 2017). The precipitation of ikaite occurs at water temperatures between 0° and 4°C (Shearman *et al.*, 1989; Bischoff *et al.*, 1993b; Benson, 1994; Huggett *et al.*, 2005; Zhou *et al.*, 2015; Brasier *et al.*, 2018; DeMott & Scholz, 2020) and with elevated concentrations of dissolved orthophosphate (Benson, 1994) or linked to hydrothermal activity (Bischoff *et al.*, 1993a,b; Ludwig *et al.*, 2006), when hot and cold fluids mix in a marine or lacustrine environment (Bischoff *et al.*, 1993b; Council & Bennett, 1993; Ludwig *et al.*, 2006; Bates *et al.*, 2010; Brasier *et al.*, 2018). Consequently, formation of calcite pseudomorphs after ikaite depends on the local water composition. A high Mg/Ca ratio transforms ikaite into aragonite, whereas a low Mg/Ca ratio results in a pseudomorphism into calcite (Purgstaller *et al.*, 2017).

In the carbonate buildups observed on the shore of both Pyramid and Winnemucca sub-basins, the presence of thinolite crystals, up to multi-decimetres in size (Fig. 7A to F), is a marker for mixing of diffuse groundwater and cold lacustrine waters (DeMott & Scholz, 2020). Thinolites are present in complex domes but absent in chimneys, in Winnemucca Lake and Pyramid Lake, which argues for diffuse groundwater rather than direct hydrothermal feeding along the vent, although their size is dependent on the calcium availability (Fig. 17 and Table 2).

Not all thinolite-containing structures are associated with complex domes in the Lahontan lacustrine system. Numerous hemispheroid domes along the Winnemucca shoreline have acicular thinolite crystals encrusted by branching microbialites (Figs 5A to D and 9A to C). They are found at the lowest water elevations and form several gentle-sloped shore belts, between 1158 masl and 1180 masl. These shorelines are dated to ages of <4 kyr (Figs 11, 15 and 16A; Adams & Rhodes, 2019). Pipes are absent and their spatial distribution is not directly related to faults or springs. During the late Holocene, the lake experienced repeated fluctuating water levels with a maximum elevation at 1199 masl due to climate variations. The late Holocene dry period resulted in a rapid decrease in water level from 1195 masl to 1155 masl between 2.8 and 1.85 kyr cal BP (Mensing *et al.*, 2013; Adams & Rhodes, 2019). At this time, the Winnemucca basin was isolated and no longer fed by Pyramid Lake. Reduced rainfall during this period of high aridity (Mensing *et al.*, 2013) did not compensate for the evaporation and resulted in increased ion concentrations. Adams & Rhodes (2019) proposed that Lake Winnemucca was an evaporitic lake when the water level was below 1183 masl, which may have supported the formation of thinolite-rich hemispheroid domes found between 1158 masl and 1180 masl along the shoreline. Therefore, thinolite may have formed in lake water high in Ca^{2+} and HCO_3^- or orthophosphate concentrations (Benson, 1984; Bischoff *et al.*, 1993a,b) resulting from intense evaporation instead of from groundwater inputs (Fig. 17, Table 2).

Despite the same climate history and similar water level fluctuations with highstands and lowstands coinciding with the Pleistocene and the Holocene (Mensing *et al.*, 2013), thinolites are absent in both Lake Bonneville and GSL (Fig. 2). The deep Lake Bonneville with steep margins and a low groundwater influx did not support the development of large-scale complex domes and columns. Great Salt Lake is comparable to the Lahontan sub-basins with respect to the physiography, but a shallow depth, high salinity (Spencer *et al.*, 1984) and low calcium and orthophosphorate concentrations did not support

ikaite precipitation and transformation into calcite (Shearman *et al.*, 1989; Bischoff *et al.*, 1993a, b). In summary, as proposed in our novel conceptual model (Fig. 17), when the proper physico-chemical conditions are met, thinolites can form either near groundwater springs or aligned along the shoreline during intense evaporation.

CONCLUSION

A comparison between the eastern (Lake Bonneville/Great Salt Lake) and western (Pyramid and Winnemucca Lakes) Great Basin provides novel insights into the controls for hybrid biotic/abiotic buildup formation during the Pleistocene and the Holocene periods. Detailed mapping and petrographic characterization of the carbonates show that:

1 The substrate plays a role in the distribution of various carbonate buildups: firm, stable and cohesive substrates (dominated by poorly altered basaltic rocks) playing physical and chemical roles in buildup development. The presence of a firm substrate depends on the preservation of watershed lithologies that register low weathering, the presence of specific sedimentological structures such as gravity flow deposits and upon previously established buildups.

2 The physiography of the basin influences the carbonate distribution: in the deep Lake Bonneville, carbonate crusts form in restricted narrow belts. Similar carbonate structures developed during a high-water level in Pyramid Lake and Winnemucca Lake upon terraces and vertical walls. The wide lateral distribution of crusts and domes in the shallow Great Salt Lake is due to a flat bottom geometry. In the Lahontan lacustrine system, the half-graben configuration determines the carbonate distribution with large complex domes on the flexural margin. This configuration also controls the distribution of the different flow pathways along groundwater springs related to faults and in front of fan-shaped delta.

3 The climate and water level fluctuations govern the distribution, the size and the morphology of the buildups: on both sides of the Great Basin, the buildups (domes and crusts) are aligned along the shorelines, and their vertical distribution reflects the fluctuations of the lake level over time. In addition, the size and morphology of the buildups are also determined by accommodation, with the taller buildups towards the basin centre, suggestive of an increase in accommodation space.

4 Tectonic controls on the carbonate buildups distribution, and the direction of groundwater flow: in the Great Salt Lakes, synsedimentary faults controlled an aligned distribution of microbialites generating local topographic highs and lows. In the Lahontan lacustrine system, the taller columns and some of the complex domes are typically aligned with the faults and fed by Ca-rich groundwaters.

5 A mass balance of Ca^{2+} shows that this reactant limits $CaCO_3$ precipitation in the water column: estimates performed for the western and eastern Great Basin show that all of the calcium supplied by the rivers is precipitated as carbonates in the GSL basin, but that the river inputs are insufficient to explain the amount of carbonate deposited in the Lahontan system, and notably in the Pyramid basin. Since the Pleistocene, an additional input is probably provided by groundwater, as indicated by the presence of large carbonate structures close to the springs and estimates of the Ca^{2+} released.

6 Groundwater chemistry influences the biotic versus abiotic carbonate precipitation processes by locally increasing the Ca^{2+} and HCO_3^- concentration: thinolites, observed only in the Lahontan lacustrine system, form when the appropriate physico-chemical conditions are met, along groundwater fed fault systems or aligned with the shoreline during intense evaporation.

In contrast to the small-scale buildups that developed along the shorelines, the large columns and complex domes in the Pyramid Lake and Winnemucca Lake are mostly determined by fault-controlled and spring-related groundwater influxes at the termination of fan-shape delta. These taller buildups result from a combined interplay of stratigraphically-related and fault-related groundwater fluxes and increasing water levels resulting from climate change. The contrast in size and distribution of the carbonate buildups at the scale of the Great Basin, opens new perspectives in the storage potential of carbon in modern times controlled by hydrothermal inputs providing ions, and enhancing carbonate production.

ACKNOWLEDGEMENTS

This work is a contribution from the SEDS team in the Biogéosciences Laboratory (UBFC, Dijon, France) to the ISITE project UB18016-BGS-IS and the project Carbostock-Envergure/OSU

THETA. We are indebted to the reviewers C. Arenas and S. Schroeder, whose comments greatly improved the manuscript. We also thank the associate editor. The authors gratefully acknowledge Raphaël Bourillot (ENSEGID, France), and Aurélie Pace (La Rochelle University), Emmanuelle Poli, Aurélien Virgone (from Total R&D), Eric Gaucher (Bern University) for stimulating discussions. We also thank Jeremy Shaw who facilitated access to Antelope Island State Park; to Cedric Bougeault for participation in the field; to Anaëlle Despiegalaere and Nicolas Marie for their contribution as master students; to Clement Bonnefoy for its expertise on GIS. We also thank Pascal Taubaty (Bourgogne Franche-Comté University, Dijon) for preparing the thin sections.

DATA AVAILABILITY STATEMENT

Data sharing is not applicable to this article as no new data were created or analyzed in this study.

REFERENCES

Adams, K.D. and **Rhodes, E.J.** (2019) Late Pleistocene to present lake-level fluctuations at pyramid and Winnemucca lakes, Nevada, USA. *Quatern. Res.*, **92**, 146–164.

Adams, K.D. and **Wesnousky, S.G.** (1999) The Lake Lahontan highstand: age, surficial characteristics, soil development, and regional shoreline correlation. *Geomorphology*, **30**, 357–392.

Allen, B.D. and **Anderson, R.Y.** (2000) A continuous, high-resolution record of late Pleistocene climate variability from the estancia basin, New Mexico. *GSA Bulletin*, **112**, 1444–1458.

Anderson, R.B., **Faulds, J.E.** and **Dering, G.M.** (2013) Preliminary geologic map of the central Lake Range, southern Fox Range, and northern Terraced Hills, Emerson Pass geothermal area, Washoe County, Nevada, Nevada Bureau of Mines and Geology, Open-File report 13-10, scale 1:24,000.

Arenas, C., **Vázquez-Urbez, M.**, **Pardo, G.** and **Sancho, C.** (2014) Sedimentology and depositional architecture of tufas deposited in stepped fluvial systems of changing slope: lessons from the Quaternary Añamaza valley (Iberian Range, Spain). *Sedimentology*, **61**(1), 133–171.

Arenas-Abad, C., **Vàzquez-Urbez, M.**, **Pardo-Tirapu, G.** and **Sancho-Marcén, C.** (2010) Fluvial and associated carbonate deposits. In: *Developments in Sedimentology. Carbonates in Continental Settings: Facies, Environments and Processes* (Eds Alonso-Zarza, A.M. and Tanner, L.H.), pp. 133–175. Elsevier, Amsterdam.

Arp, G., **Helms, G.**, **Karlinska, K.**, **Schumann, G.**, **Reimer, A.**, **Reitner, J.** and **Trichet, J.** (2012) Photosynthesis versus exopolymer degradation in the formation of microbialites on the atoll of Kiritimati, Republic of Kiribati, Central Pacific. *Geomicrobiol. J.*, **29**, 29–65.

Arp, G., **Thiel, V.**, **Reimer, A.**, **Michaelis, W.** and **Reitner, J.** (1999) Biofilm exopolymers control microbialite formation at thermal springs discharging into the alkaline pyramid Lake, Nevada, USA. *Sed. Geol.*, **126**, 159–176.

Baskin, R.L. and **Allen, D.V.** (2005) *Bathymetric Map of the South Part of Great Salt Lake, Utah, Scientific Investigations Map 2894*. U.S. Geological Survey, Salt Lake City.

Baskin, R.L., **Della Porta, G.** and **Wright, V.P.** (2021) Characteristics and controls on the distribution of sublittoral microbial bioherms in great salt Lake, Utah: implication for understanding microbialites development. *Depos. Rec.*, **8**, 39–66.

Baskin, R.L., **Driscoll, N.** and **Wright, V.P.** (2011) Lacustrine microbialites in Great Salt Lake: life in a dead lake. *Am. Assoc. Petrol. Geol. Ann. Convent. Abs.*, **13** Search and Discovery article #90153.

Baskin, R.L. and **Turner, J.** (2006) *Bathymetric Map of the North Part of Great Salt Lake, Utah, Scientific Investigations Map 2894*. U.S. Geological Survey, Reston.

Bates, A.E., **Lee, R.W.**, **Tunnicliffe, V.** and **Lamare, M.D.** (2010) Deep-sea hydrothermal vent animals seek cool fluids in a highly variable thermal environment. *Nat. Commun.*, **1**, 14–19.

Benson, L.V. (1984) *Hydrochemical Data for the Truckee River Drainage System, California and Nevada*. U.S. Geological Survey, Denver Colorado, United States, Open-File Report 84-440, 35 pp.

Benson, L.V. (1994) Carbonate deposition, pyramid Lake subbasin, Nevada: 1. Sequence of formation and elevational distribution of carbonate deposits (Tufas). *Palaeogeogr. Palaeoclimatol. Palaeoecol.*, **109**, 55–87.

Benson, L.V., **Currey, D.**, **Lao, Y.** and **Hostetler, S.** (1992) Lake-size variations in the Lahontan and Bonneville basins between 13,000 and 9,000 ^{14}C yr BP. *Palaeogeogr. Palaeoclimatol. Palaeoecol.*, **95**, 19–32.

Benson, L.V., **Hattori, E.M.**, **Southon, J.** and **Aleck, B.** (2013a) Dating North America's oldest petroglyphs, Winnemucca Lake subbasin, Nevada. *J. Archaeol. Sci.*, **40**, 4466–4476.

Benson, L., **Kashgarian, M.** and **Rubin, M.** (1995) Carbonate deposition, pyramid Lake subbasin, Nevada: 2. Lake levels and polar jet stream positions reconstructed from radiocarbon ages and elevations of carbonates (tufas) deposited in the Lahontan basin. *Palaeogeogr. Palaeoclimatol Palaeoecol.*, **117**, 1–30.

Benson, L.V. and **Leach, D.L.** (1979) Uranium transport in the Walker River basin, California and Nevada. *J. Geochem. Explor.*, **11**, 227–248.

Benson, L.V. and **Mifflin, M.D.** (1986) *Reconnaissance Bathymetry of Basins Occupied by Pleistocene Lake Lahontan, Nevada and California*. US Geological Survey Water Resources Investigations, Denver Colorado, Report 85–4262, 14 pp.

Benson, L. and **Peterman, Z.** (1996) Carbonate deposition, pyramid Lake subbasin, Nevada: 3. The use of ^{87}Sr values in carbonate deposits (tufas) to determine the hydrologic state of paleolake systems. *Palaeogeogr. Palaeoclimatol. Palaeoecol.*, **119**, 201–213.

Benson, L.V., **Smoot, J.P.**, **Lund, S.P.**, **Mensing, S.A.**, **Foit, F.F.** and **Rye, R.O.** (2013b) Insights from a synthesis of old and new climate-proxy data from the pyramid and Winnemucca lake basins for the period 48 to 11.5 cal ka. *Quatern. Int.*, **310**, 62–82.

Benson, L., **White, L.D.** and **Rye, R.** (1996) Carbonate deposition, pyramid Lake subbasin, Nevada: 4. Comparison of the stable isotope values of carbonate deposits (tufas) and the Lahontan lake-level record. *Palaeogeogr. Palaeoclimatol. Palaeoecol.*, **122**, 45–76.

Bischoff, J.L., **Fitzpatrick, J.A.** and **Rosenbauer, R.J.** (1993a) The solubility and stabilization of ikaite ($CaCO_3{\cdot}6H_2O$) from 0° to 25°C: environmental and paleoclimatic implications for thinolite tufa. *J. Geol.*, **101**, 21–33.

Bischoff, J.L., **Stine, S.**, **Rosenbauer, R.J.**, **Fitzpatrick, J.A.** and **Stafford, T.W.** (1993b) Ikaite precipitation by mixing of shoreline springs and Lake water, mono lake, California, USA. *Geochim. Cosmochim. Acta*, **57**, 3855–3865.

Blair, T.C. (1999) Sedimentary processes and facies of the waterlaid anvil spring canyon alluvial fan, Death Valley, California. *Sedimentology*, **46**, 913–940.

Bonham, H.F., Jr. (1969) Geology and mineral deposits of Washoe and Storey Counties, Nevada, with a section on Industrial rock and mineral deposits by Papke, K.G.: Nevada Bureau of Mines and Geology Bulletin 70, 140 pp.

Bouton, A., **Vennin, E.**, **Amiotte-Suchet, P.**, **Thomazo, C.**, **Sizun, J.**, **Virgone, A.**, **Gaucher, E.C.** and **Visscher, P.T.** (2020) Prediction of the calcium carbonate budget in a sedimentary basin: a "source-to-sink" approach applied to great salt Lake, Utah, USA. *Basin Res.*, **32**, 1005–1034.

Bouton, A., **Vennin, E.**, **Boulle, J.**, **Pace, A.**, **Bourillot, R.**, **Thomazo, C.**, **Brayard, A.**, **Désaubliaux, G.**, **Goslar, T.**, **Yokoyama, Y.**, **Dupraz, C.** and **Visscher, P.T.** (2016a) Linking the distribution of microbial deposits from the great salt Lake (Utah, USA) to tectonic and climatic processes. *Biogeosciences*, **13**, 5511–5526.

Bouton, A., **Vennin, E.**, **Mulder, T.**, **Pace, A.**, **Bourillot, R.**, **Thomazo, C.**, **Brayard, A.**, **Goslar, T.**, **Buoncristiani, J.-F.**, **Désaubliaux, G.** and **Visscher, P.T.** (2016b) Enhanced development of lacustrine microbialites on gravity flow deposits, great salt Lake, Utah, USA. *Sed. Geol.*, **341**, 1–12.

Brasier, A., **Wacey, D.**, **Rogerson, M.**, **Guagliardo, P.**, **Saunders, M.**, **Kellner, S.**, **Mercedes-Martin, R.**, **Prior, T.**, **Taylor, C.**, **Matthews, A.** and **Reijmer, J.** (2018) A microbial role in the construction of mono Lake carbonate chimneys? *Geobiology*, **16**, 1–16.

Burne, R.V. and **Moore, L.S.** (1987) Microbialites: organosedimentary deposits of benthic microbial communities. *Palaios*, **2**, 241–254.

Chafetz, H.S. and **Buczynski, C.** (1992) Bacterially induced lithification of microbial mats. *Palaios*, **7**, 277–293.

Chafetz, H.S., **Utech, N.M.** and **Fitzmaurice, S.P.** (1991) Differences in the $\delta^{18}O$ and ^{13}C signatures of seasonal laminae comprising travertine stromatolites. *J. Sed. Res.*, **61**, 1015–1028.

Chambers, J.C. and **Miller, J.R.** (2011) *Geomorphology, Hydrology, and Ecology of Great Basin Meadow Complexes - Implications for Management and Restoration (No. RMRS-GTR- 258).* U.S. Department of Agriculture, Forest Service, Rocky Mountain Research Station, Ft. Collins, CO, 125 pp.

Cohen, A.B. (2021) *Particle-Associated Microbial Processes in Permanently Anoxic Fayetteville Green Lake, Fayetteville, NY: A Window into the Mid-Proterozoic Ocean.* PhD Thesis. Stony Brook University, State University of New York, New York, 224 pp.

Coolbaugh, M.F., **Faulds, J.E.**, **Kratt, C.**, **Oppliger, G.L.**, **Shevenell, L.**, **Calvin, W.M.**, **Ehni, W.J.** and **Zehner, R.E.** (2007) Geothermal potential of the pyramid Lake Paiute reservation, Nevada, USA: evidence of previously unrecognized moderate- temperature (150–170°C) geothermal systems. *Geoth. Res. Coun. Trans.*, **30**, 59–67.

Coolbaugh, M.F., **Lechler, P.**, **Sladeck, C.** and **Kratt, C.** (2009) Carbonate tufa columns as exploration guides for geothermal systems in the Great Basin. *Geoth. Res. Coun. Trans.*, **33**, 461–466.

Coolbaugh, M., **Lechler, P.**, **Sladek, C.** and **Kratt, C.** (2010) Lithium in tufas of the Great Basin: exploration implications for geothermal energy and lithium resources. *Geoth. Res. Coun. Trans.*, **34**, 521–526.

Council, T.C. and **Bennett, P.C.** (1993) Geochemistry of ikaite formation at mono Lake, California: implications for the origin of tufa mounds. *Geol. Soc. Am. Bull.*, **21**, 971–974.

Cukur, D., **Krastel, S.**, **Çağatay, M.N.**, **Damcı, E.**, **Meydan, A.F.** and **Kim, S.-P.** (2015) Evidence of extensive carbonate mounds and sublacustrine channels in shallow waters of Lake Van, eastern Turkey, based on high-resolution chirp subbottom profiler and multibeam echosounder data. *Geo-Mar. Lett.*, **35**, 329–340.

Dekov, V.M., **Egueh, N.M.**, **Kamenov, G.D.**, **Bayon, G.**, **Lalonde, S.V.**, **Schmidt, M.**, **Liebetrau, V.**, **Munnik, F.**, **Fouquet, Y.**, **Tanimizu, M.**, **Awaleh, M.O.**, **Guirreh, I.** and **Le Gall, B.** (2014) Hydrothermal carbonate chimneys from a continental rift (Afar rift): mineralogy, geochemistry, and mode of formation. *Chem. Geol.*, **387**, 87–100.

Della Porta, G. (2015) Carbonate build-ups in lacustrine, hydrothermal and fluvial settings: comparing depositional geometry, fabric types and geochemical signature. In: *Microbial Carbonates in Space and Time: Implications for Global Exploration and Production* (Eds Bosence, D.W.J., Gibbons, K.A., Le Heron, D.P., Morgan, W.A., Pritchard, T. and Vining, B.A.), *Geol. Soc. Lond. Spec. Publ*, **418**, 17–68.

DeMott, L.M., **Napieralski, S.A.**, **Junium, C.K.**, **Teece, M.** and **Scholz, C.A.** (2019a) Microbially influenced lacustrine carbonates: a comparison of late quaternary Lahontan tufa and modern thrombolite from Fayetteville Green Lake, NY. *Geobiology*, **18**, 93–112.

DeMott, L. and **Scholz, C.A.** (2020) Lacustrine carbonate tufa facies of Winnemucca dry Lake Basin, Nevada, USA. *J. Sed. Res.*, **90**, 1804–1828.

DeMott, L.M., **Scholz, C.A.** and **Junium, C.K.** (2019b) 8200-year growth history of a Lahontan-age lacustrine tufa deposit. *Sedimentology*, **66**, 2169–2190.

Drakos, P.S. and **Faulds, J.E.** (2013) Preliminary Geologic Map of the Southern Lake Range, Washoe County, Nevada. Text accompanying Nevada Bureau of Mines and Geology Open-Fil, 13-11, scale 1:24,000, pp. 1–5.

Dupraz, C., **Reid, R.P.**, **Braissant, O.**, **Decho, A.W.**, **Norman, R.S.** and **Visscher, P.T.** (2009) Processes of carbonate precipitation in modern microbial mats. *Earth Sci. Rev.*, **9**, 141–162.

Dupraz, C., **Reid, R.P.**, **Visscher, P.T.**, **Reitner, J.** and **Thiel, V.** (2011) Microbialites, modern. In: *Encyclopedia of Geobiology* (Eds Reitner, J. and Thiel, V.), pp. 653–654. Encyclopedia of Earth Science Series, Berlin, Springer.

Dupraz, C. and **Visscher, P.T.** (2005) Microbial lithification in marine stromatolites and hypersaline mats. *Trends Microbiol.*, **13**, 429–438.

Eisses, A.K., **Kell, A.**, **Kent, G.M.**, **Driscoll, N.W.**, **Baskin, R.L.**, **Smith, K.D.**, **Karlin, R.E.**, **Louie, J.N.** and **Pullamanappallil, S.K.** (2015) New constraints on fault architecture, slip rates, and strain partitioning beneath pyramid Lake. *Geosphere*, **11**, 683–704.

Faulds, J.E. and **Hinz, N.H.** (2015) Favorable Tectonic and Structural Settings of Geothermal Systems in the Great Basin Region, Western USA: Proxies for Discovering Blind Geothermal Systems. Presented at the Proceedings of the World Geothermal Congress, Melbourne, Australia, pp. 19–25.

Forrest, M.J., **Ledesma-Vazquez, J.**, **Ussler, W., III**, **Kulongoski, J.T.**, **Hilton, D.R.** and **Green, H.G.** (2005) Gas geochemistry of shallow submarine hydrothermal vent

associated with the El Requeson fault zone, Bahia Concepcion, Baja California Sur, México. *Chem. Geol.*, **224**, 82–95.

Forrest, M.J. and **Melwani, A.** (2003) *Ecological Consequences of Shallow-Water Hydrothermal Venting Along the El Requeson Fault Zone, Bahia Concepcion, BCS, Mexico*, pp. 577–578. Geological Society of America Abstracts with Programs, Seattle.

Godsey, H.S., **Oviatt, C.G.**, **Miller, D.M.** and **Chan, M.A.** (2011) Stratigraphy and chronology of offshore to nearshore deposits associated with the Provo shoreline, Pleistocene Lake Bonneville, Utah. *Palaeogeogr. Palaeoclimatol. Palaeoecol.*, **310**, 442–450.

Gradziński, M. (2010) Factors controlling growth of modern tufa: results of a field experiment. *J. Geol. Soc London, Spec Public*, **336**, 143–191.

Gwynn, J.W. (1996) Commonly Asked Questions about Utah's Great Salt Lake and Ancient Lake Bonneville, Public Information Series. Edited by: Survey, U. G., 22 pp.

Hahl, D.C. and **Langford, R.H.** (1964) *Dissolved-Mineral Inflow to Great Salt Lake and Chemical Characteristics of the Salt Lake Brine, Part II: Technical Report*. Utah Geological and Mineralogical Survey Water-Resources Bulletin 3-II, Salt Lake City, UT, 40 pp.

Hammond, W.C., **Blewitt, G.** and **Kreemer, C.** (2011) Block modeling of crustal deformation of the northern Walker lane and basin and range from GPS velocities. *J. Geophys. Res.*, **116**, 1–28.

Hofmann, B.A. and **Farmer, J.D.** (2000) Filamentous fabrics in low-temperature mineral assemblages: are they fossil biomarkers? Implications for the search for a sub-surface fossil record on the early earth and Mars. *Planet. Space Sci.*, **48**, 1077–1086.

Huggett, J.M., **Schultz, B.P.**, **Shearman, D.J.** and **Smith, A.J.** (2005) The petrology of ikaite pseudomorphs and their diagenesis. *Proc. Geol. Assoc.*, **116**, 207–220.

Jahnert, R.J. and **Collins, L.B.** (2013) Controls on microbial activity and tidal flat evolution in Shark Bay, Western Australia. *Sedimentology*, **60**, 1071–1099.

Kelts, K. and **Talbot, M.** (1990) Lacustrine carbonates as geochemical archives of environmental change and biotic/abiotic interactions. In: *Large Lakes* (Eds Tilzer, M. and Serruya, C.), pp. 288–315. Springer, Berlin, Heidelberg.

Kratt, C., **Calvin, W.M.** and **Coolbaugh, M.F.** (2010) Mineral mapping in the pyramid Lake basin: hydrothermal alteration, chemical precipitates and geothermal energy potential. *Remote Sens. Environ.*, **114**, 2297–2304.

Lindsay, M.R., **Dunham, E.C.** and **Boyd, E.S.** (2020) Microbialites of great salt Lake. In: *Great Salt Lake Biology* (Eds Baxter, B. and Butler, J.), pp. 87–118. Springer, Cham.

Ludwig, K.A., **Kelley, D.S.**, **Butterfield, D.A.**, **Nelson, B.K.** and **Früh-Green, G.** (2006) Formation and evolution of carbonate chimneys at the lost City hydrothermal field. *Geochim. Cosmochim. Acta*, **70**, 3625–3645.

Machette, M.N., **Personius, S.F.** and **Nelson, A.R.** (1992) Paleoseismology of the Wasatch fault zone—a summary of recent investigations, interpretations, and conclusions. In: *Assessment of Regional Earthquake Hazards and Risk along the Wasatch Front, Utah* (Eds Gori, P.L. and Hays, W.W.), *U. S. Geological Survey Professional Paper*, **1500-A**, A1–A71.

Madsen, D.B., **Rhode, D.**, **Grayson, D.K.**, **Broughton, J.M.**, **Livingston, S.D.**, **Hunt, J.**, **Quade, J.**, **Schmitt, D.N.** and **Shaver, M.W.** (2001) Late quaternary environmental change in the Bonneville basin, western USA. *Palaeogeogr. Palaeoclimatol. Palaeoecol.*, **167**, 243–271.

Matsubara, Y. and **Howard, A.D.** (2009) A spatially explicit model of runoff, evaporation, and lake extent: application to modern and late Pleistocene lakes in the Great Basin region, western United States. *Water Resources Research*, **45**, W06425.

McKenzie, J.A. and **Eberli, G.P.** (1985) Late Holocene Lake-level fluctuations of the great salt lake (Utah) as deduced form oxygen isotope and carbonate contents of cored sediments. In: *Proceedings of Workshop on Problems of and Prospects for Predicting Great Salt Lake Levels* (Eds Kay, P.A. and Diaz, H.F.), pp. 25–39. Center Publ. Affairs Admin., Univ. Utah, Utah.

Mensing, S.A., **Sharpe, S.E.**, **Tunno, I.**, **Sada, D.W.**, **Thomas, J.M.**, **Starratt, S.** and **Smith, J.** (2013) The late Holocene dry period: multiproxy evidence for an extended drought between 2800 and 1850 cal yr BP across the central Great Basin, USA. *Quatern. Sci. Rev.*, **78**, 266–282.

Mohammad, S. and **Tempel, R.N.** (2019) Arsenic in the waters and sediments of the humboldt river, north-central Nevada, USA: hydrological and mineralogical investigation. *Environmental Earth Sciences*, **78**(17), 1–16.

Murchison, S.B. (1989) *Fluctuation History of Great Salt Lake, Utah, During the Last 13,000 Years*. Ph.D. Thesis. University of Utah, Salt Lake City, UT, 157 pp.

Oviatt, C.G. (1997) Lake Bonneville fluctuations and global climate change. *Geology*, **25**, 155–158.

Oviatt, C.G. (2015) Chronology of Lake Bonneville, 30,000 to 10,000 yr B.P. *Quatern. Sci. Rev.*, **110**, 166–171.

Oviatt, C.G., **Currey, D.R.** and **Sack, D.** (1992) Radiocarbon chronology of Lake Bonneville, eastern Great Basin, USA. *Palaeogeogr. Palaeoclimatol. Palaeoecol.*, **99**, 225–241.

Oviatt, C.G. and **Nash, B.** (2014) The pony express basaltic ash: a stratigraphic marker in late Pleistocene Lake Bonneville deposits, Utah. *Utah Geol. Surv.*, **14-1**, 10.

Pace, A., **Bourillot, R.**, **Bouton, A.**, **Vennin, E.**, **Galaup, S.**, **Bundeleva, I.**, **Patrier, P.**, **Dupraz, C.**, **Thomazo, C.**, **Sansjofre, P.**, **Yokoyama, Y.**, **Franceschi, M.**, **Anguy, Y.**, **Pigot, L.**, **Virgone, A.** and **Visscher, P.T.** (2016) Microbial and diagenetic steps leading to the mineralisation of great salt Lake microbialites. *Sci. Rep.*, **6**, 1–12.

Patrickson, S.J., **Sack, D.**, **Brunelle, A.R.** and **Moser, K.A.** (2010) Late Pleistocene to early Holocene lake level and paleoclimate insights from Stansbury Island, Bonneville basin, Utah. *Quatern. Res.*, **73**, 237–246.

Pedley, H.M. (2000) Ambient temperature freshwater microbial tufas. In: *Microbial Sediments* (Eds Riding, R. and Awramik, S.M.), pp. 179–186. Springer, Berlin.

Pedley, M. (2014) The morphology and function of thrombolytic calcite precipitating biofilms: a universal model derived from freshwater mesocosm experiments. *Sedimentology*, **61**, 22–40.

Pedley, H.M. and **Rogerson, M.** (2010) Introduction to tufas and speleothems. *J. Geol. Soc.*, **336**, 1–5.

Prol-Ledesma, R.M., **Canet, C.**, **Torres-Verra, M.A.**, **Forrest, M.J.** and **Armienta, M.A.** (2004) Vent fluid chemistry in Bahia conception coastal submarine hydrothermal system, Baja California Sur, Mexico. *J. Volcanol. Geoth. Res.*, **137**, 311–328.

Purgstaller, B., **Dietzel, M.**, **Baldermann, A.** and **Mavromatis, V.** (2017) Control of temperature and aqueous Mg^{2+}/Ca^{2+} ratio on the (trans-)formation of ikaite. *Geochim. Cosmochim. Acta*, **217**, 128–143.

Reheis, M.C., **Adams, K.D.**, **Oviatt, C.G.** and **Bacon, S.N.** (2014) Pluvial lakes in the Great Basin of the western United States-a view from the outcrop. *Quatern. Sci. Rev.*, **97**, 33–57.

Richardson, G.B. (1906) *Underground Water in the Valleys of Utah Lake and Jordan River, Utah*. Water Supply Paper, Washington, DC, 93 pp.
Riding, R. (2000) Microbial carbonates: the geological record of calcified bacterial–algal mats and biofilms. *Sedimentology*, **47**, 179–214.
Riding, R. and **Virgone, A.** (2020) Hybrid carbonates:in situ abiotic, microbial and skeletal co-precipitates. *Earth Sci. Rev.*, **208**, 103300.
Roche, A. (2020) *Dépôts carbonates microbiens en domaine lacustre et fluviatile: Fabriques et facteurs de Contrôle*. Unpublished PhD Thesis. University of Bourgogne Franche-Comté, Dijon, 360 pp.
Roche, A., **Vennin, E.**, **Bouton, A.**, **Olivier, N.**, **Wattinne, A.**, **Bundeleva, I.**, **Deconinck, J.-F.**, **Virgone, A.**, **Gaucher, E.C.** and **Visscher, P.T.** (2018) Oligo-Miocene lacustrine microbial and metazoan buildups from the Limagne Basin (French massif central). *Palaeogeogr., Palaeoclimatol. Palaeoecol.*, **504**, 34–59.
Roche, A., **Vennin, E.**, **Bundeleva, I.**, **Bouton, A.**, **Payandi-Rolland, D.**, **Amiotte-Suchet, P.**, **Gaucher, E.C.**, **Courvoisier, H.** and **Visscher, P.T.** (2019) The role of the substrate on the mineralization potential of microbial mats in a modern freshwater river (Paris Basin, France). *Minerals*, **9**, 1–33.
Schaegis, J.C., **Rime, V.**, **Kidane, T.**, **Mosar, J.**, **Gebru, E.F.**, **Atnafu, B.** and **Foubert, A.** (2021) Novel bathymetry of Lake Afdera reveals fault structures and volcano-tectonic features of an incipient transform zone (Afar, Ethiopia). *Front. Earth Sci.*, **9**, 706643.
Schopf, J.W., **Kudryavtsev, A.B.**, **Czaja, A.D.** and **Tripathi, A.B.** (2007) Evidence of Archean life: stromatolites and microfossils. *Precambrian Res.*, **158**, 141–155.
Schuster, M. and **Nutz, A.** (2018) Lacustrine wave-dominated clastic shorelines: modern to ancient littoral landforms and deposits from the Lake Turkana Basin (east African rift system, Kenya). *J. Paleolimnol.*, **59**, 221–243.
Shapiro, R.S. (2000) A comment on the systematic confusion of thrombolites. *Palaios*, **15**, 166–169.
Shearman, D.J., **McGugan, A.**, **Stein, C.** and **Smith, A.J.** (1989) Ikaite, CaCO3.6H2O, precursor of the thinolites in the quaternary tufas and tufa mounds of the Lahontan and mono Lake basins, western United States. *Geol. Soc. Am. Bull.*, **10**, 913–917.
Smith, R.B. and **Bruhn, R.L.** (1984) Intraplate extensional tectonics of the eastern basin-range: inferences on structural style from seismic reflection data, regional tectonics, and thermal-mechanical models of brittle-ductile deformation. *J. Geophys. Res. Solid Earth*, **89B7**, 5733–5762.
Spencer, R., **Baedecker, M.J.**, **Eugster, H.P.**, **Forester, R.M.**, **Goldhaber, M.B.**, **Jones, B.F.**, **Kelts, K.**, **McKenzie, J.**, **Madsen, D.B.**, **Rettig, S.L.**, **Rubin, M.** and **Bowser, C.J.** (1984) Great salt Lake, and precursors, Utah: the last 30,000 years. *Contrib. Mineral. Petrol.*, **86**, 321–334.
Stewart, J.H. (1971) Basin and range structure: a system of horsts and grabens produced by deep-seated extension. *Geol. Soc. Am. Bull.*, **82**, 1019–1044.
Stewart, J.H., **Carlson, J.E.** and **Johannesen, D.C.** (1982) Geologic Map of the Walker Lake 1 by 2 Quadrangle. Miscellaneous Field Studies Map 1382-A.
Thompson, J.B., **Ferris, F.G.** and **Smith, D.A.** (1990) Geomicrobiology and sedimentology of the mixolimnion and chemocline on Fayetteville Green Lake, New York. *Palaios*, **5**, 52–75.
Trampe, E.C.L., **Larsen, J.E.N.**, **Glaring, M.A.**, **Stougaard, P.S.** and **Kühl, M.** (2016) *In situ* dynamics of O_2, pH, light, and photosynthesis in ikaite tufa columns (Ikka Fjord, Greenland)—a unique microbial habitat. *Front. Microbiol.*, **7**, 1–13.
Van Buer, N. (2012) *Preliminary Geologic Map of the Sahwave and Nightingale Ranges, Churchill, Pershing, and Washoe Counties, Nevada. Open File Report 12-2, 1:62,500 scale*. Nevada Bureau of Mines and Geology, Reno, NV.
Vanden Berg, M.D. (2019) Domes, rings, ridges, and polygons: characteristics of microbialites from Utah's great salt Lake. *Sed. Record*, **17**, 4–10.
Vennin, E., **Bouton, A.**, **Bourillot, R.**, **Pace, A.**, **Roche, A.**, **Brayard, A.**, **Thomazo, C.**, **Virgone, A.**, **Gaucher, E.C.**, **Desaubliaux, G.** and **Visscher, P.T.** (2019) The lacustrine microbial carbonate factory of the successive Lake Bonneville and great salt Lake, Utah, USA. *Sedimentology*, **66**, 165–204.
Vennin, E., **Bouton, A.**, **Roche, A.**, **Gérard, E.**, **Bundeleva, I.**, **Boussagol, P.**, **Wattinne, A.**, **Kolodka, C.**, **Gaucher, E.**, **Virgone, A.** and **Visscher, P.T.** (2021) The Limagne Basin: a journey through modern and fossil microbial deposits. *Bull. Soc. Géol. Fr.*, **192**, 1–41.
Vice, G.S., **Faulds, J.E.**, **Ehni, W.J.** and **Coolbaugh, M.F.** (2007) Structural controls of a blind geothermal system in the northern pyramid Lake area, northwestern Nevada. *Geothermal Res. Council Transac.*, **31**, 133–137.
Visher, F.N. (1957) Geology and Ground-Water Resources of Quinn River Valley, Humboldt County, Nevada, State of Nevada Office of State Engineer. *Water Resources Bull.*, **15**, 56.
Visscher, P.T., **Gallagher, K.L.**, **Bouton, A.**, **Vennin, E.**, **Thomazo, C.**, **White, R.A., III** and **Burns, B.P.** (2022) Treatise online no.163: part B, volume 1, chapter 3: microbial mats. *Treatise Online*.
Visscher, P.T., **Reid, R.P.**, **Bebout, B.M.**, **Hoeft, S.E.**, **Macintyre, I.G.** and **Thompson, J.A., Jr.** (1998) Formation of lithified micritic laminae in modern marine stromatolites (Bahamas): the role of sulfur cycling. *Am. Mineral.*, **83**, 1482–1491.
Wesnousky, S.G. (2005) The San Andreas and Walker lane fault systems, western North America: transpression, transtension, cumulative slip and the structural evolution of a major transform plate boundary. *J. Struct. Geol.*, **27**, 1505–1512.
Zeebe, R.E. (2012) History of seawater carbonate chemistry, atmospheric CO_2, and ocean acidification. *Annu. Rev. Earth Planet. Sci.*, **40**, 141–165.
Zhou, X., **Lu, Z.**, **Rickaby, R.E.M.**, **Domack, E.W.**, **Wellner, J.S.** and **Kennedy, H.A.** (2015) Ikaite abundance controlled by porewater phosphorus level: potential links to dust and productivity. *J. Geol.*, **123**, 269–281.

Manuscript received 17 March 2022; revision accepted 8 December 2022

Supporting Information

Additional information may be found in the online version of this article:

Appendix S1. Calcium inputs and storage: hydrological and carbonate sedimentation.
Appendix S2. Table showing the main estimates of inputs and storage of calcium in the Lahontan lacustrine system since 10 ka, and between 48 ka and 14 ka.